A VERTICAL VEGETATION STRUCTURE MODEL OF THE EARTH

Hui Zhang[*†] University of Copenhagen
Nico Lang[*†] University of Copenhagen
Mikolaj Mazurczyk University of Copenhagen
Stefan Oehmcke University of Rostock
Ke Huang University of Copenhagen
Martin Brandt University of Copenhagen
Rasmus Fensholt University of Copenhagen
Ankit Kariryaa University of Copenhagen
Christian Igel[†] University of Copenhagen

October 7, 2026

ABSTRACT

Knowing the global distribution of vegetation structure is an essential prerequisite to better quantify, model, and manage carbon, water, energy, and biodiversity in the Earth system[1–3]. Despite its recognized importance, vertical structure measurements remain sparse at global scales, limiting our understanding of the links between structure and ecosystem functions and resilience[4–6]. Here we present global vertical vegetation structure data for the year 2020 at 10 m spatial resolution. A deep learning approach was developed to combine satellite images from Sentinel-2 with 178 million sparse height profile measurements from the GEDI spaceborne LiDAR mission. While prior work has focused on modeling canopy top height or other scalar descriptors of structure[5, 7–9], we provide a detailed global representation of the full vertical vegetation structure. Not only does this improve canopy top height estimates by up to 37% compared to commonly used top height proxies, but more importantly, the vertical structure estimates reveal conservation-relevant differences in canopy organization, lower-canopy structure, and canopy closure that are otherwise compressed or missed by top height and scalar complexity products. For example, we find that our full profile data improve the identification of natural forests by 42% relative to using canopy top height alone, likely being a result of the improved sensitivity to fine-scale structural signatures associated with anthropogenic disturbance, including structural changes caused by forest degradation or selective logging. By revealing subtle signatures associated with forest management and potential degradation, the presented vertical structure model provides a foundation for implementing global conservation initiatives[10–12] and advancing early warning systems in ecosystem monitoring. [3]

Keywords vegetation structure, forest naturalness, canopy height, GEDI, deep learning, uncertainty quantification

1 Introduction

Vegetated land provides a central basis for human and animal life[13, 14], often indirectly by regulating the climate at local and global scales, providing food, regulating the watershed, and conserving biodiversity. Intact vegetation ecosystems can reduce the destructive impact of severe weather events and climate change[15], for example, by lowering the risk of soil erosion and land-slides, or by acting as a buffer against hurricanes, storm surges, and avalanches.

[*]Corresponding authors: huzh@di.ku.dk, nila@di.ku.dk
[†]These authors contributed equally to this work.
[3]The data can be inspected and downloaded globally via our data viewer: `https://huizhml.github.io/map-explorer/`

Preprint status. This manuscript is an EarthArxiv preprint and has been submitted to a journal for peer review and possible publication. Subsequent versions of this manuscript may differ from the present version.

Nevertheless, intact ecosystems are under immense pressure due to human activities[16] often associated with the production of commodities such as palm oil, cocoa, soybeans, and cattle[17, 18]. Even formally protected areas are impacted[19] and about one-third of global protected areas are under intense human pressure[20]. The urgency of adapting to a changing climate and avoiding biodiversity collapse[21] led to several international environmental initiatives to preserve the remaining intact ecosystems and to reverse degraded habitats to a natural state. Examples include the "30 by 30" commitment that protects 30% of the world's lands, oceans, and freshwaters by the year 2030[11], and the European Union (EU) Deforestation Regulation (EUDR)[12], which aims to limit deforestation caused by the major agricultural commodities sold in the EU.

A crucial step towards implementing such global conservation targets on land is to quantify the conservational value of vegetation ecosystems to guide resources towards protecting the most valuable ecosystems[1–3]. Quantifying this conservational value is challenging as we need to account for a multitude of criteria including carbon stocks[22], biodiversity[23], and the naturalness of ecosystems[24]. The conservation and reforestation of degraded forests is discussed as a mechanism to sequester carbon from the atmosphere, but high uncertainties of estimated carbon stock potentials[25] and ecosystem services remain a challenge[25]. In general, monitoring ecosystem functions such as ecosystem productivity and carbon-use efficiency is pivotal to understand how ecosystems respond to anthropogenic drivers and a changing climate[6].

Vertical vegetation structure is a key three-dimensional property that allows to model aboveground carbon stocks, biodiversity, and the naturalness of ecosystems[5, 26, 27], and a dominant factor explaining variation in ecosystem function[6]. In practice, however, most studies have relied on canopy top height or individual structural complexity indices as proxies for vertical structure[28, 29], largely because spatially continuous measurements of the structure have been scarce at scale. Such scalar summaries compress the vertical organization of the canopy into a single value, leaving lower strata under-represented and reducing sensitivity to fine-scale, three-dimensional structural signatures caused by natural processes or human activity. Selective logging, for example, removes upper-canopy elements and reduces the thermal buffering that keeps understory microclimate cool on hot days. Such structural change reshapes the vertical profile and the ecosystem services of intact natural forests, yet remains largely invisible in canopy top height estimates. To better understand the human drivers influencing forest structure and to support the management of protected-areas, we need vegetation structure data that are globally consistent, timely, and of a high spatial resolution that resolves human activities such as development of forest tracks and selective logging[19].

Today, there is no single satellite sensor that can measure high-resolution vertical vegetation structure at global scales. However, remote sensing research has played a central part in developing approaches for fusing data from different space missions to create derived data products. On the one hand, dedicated laser scanner instruments like the Global Ecosystem Dynamics Investigation (GEDI) have advanced the availability of sparse global-scale vertical structure measurements[4]. As a sampling mission, GEDI yields spatially sparse measurements, and the derived products provide only scalar summaries of structure[5, 30], rather than a spatially continuous full vertical profile. On the other hand, optical satellite missions like Sentinel-2 or Landsat provide dense coverage at spatial resolutions up to 10 m with revisit times of five days, but do not provide a direct measurement of vertical vegetation structure. Modeling vegetation parameters using both types of sensors provides a promising pathway to overcome the limitations of each sensor alone. The progress of artificial intelligence (AI) and modern machine learning methods has led to advanced canopy height products[8, 9, 31] and global structural complexity maps[5, 30], but the state of the art of the characterization of vertical structure remains limited by capturing only a few statistics of the structure[30] and by covering few geographic regions[32].

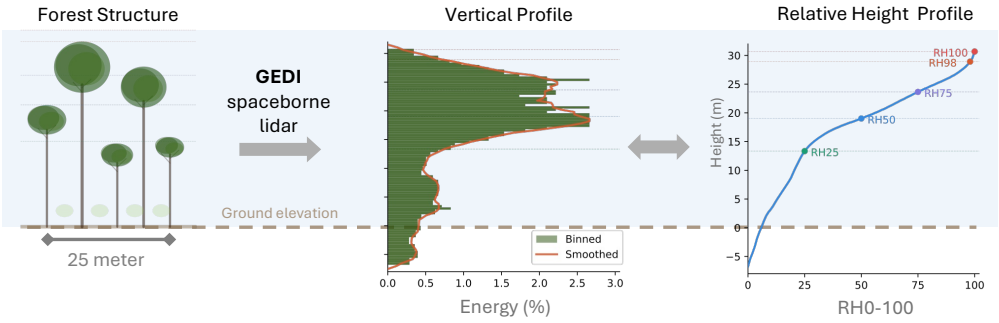


Figure 1: The GEDI sensor measures sparse vertical profiles of vegetation structure within a 25m footprint. This data is represented as 101 Relative Height (RH) metrics, each describing the height above ground at which a certain percentage of the laser energy is returned.

Here, we present a deep learning approach that combines Sentinel-2 and GEDI data to model the vertical structure of vegetation globally with 10 m spatial resolution, and thus, goes beyond the state of the art marked by single statistics as proxies for the vegetation structure. We extend the established concept of *canopy height models* (CHM), that is, the rastered data of vegetation height above ground, to the concept of *vertical structure model* (VSM) to represent the full three-dimensional vegetation structure. Concretely, the VSM describes each 10 m pixel by a full RH profile with 101 relative height metrics (RH0-RH100, see Fig. 1) with calibrated prediction intervals, characterizing how vegetation is distributed from the ground to the canopy top. The presented VSM is a three-dimensional data cube that covers the entire landmass of the Earth with unprecedented spatial resolution and coverage. While this study focuses on establishing a reference of the global distribution of vegetation structure for the year 2020, in principle, our methodology only requires a single cloud-free satellite image to compute the VSM. Since a new Sentinel-2 image is available at any location globally, at least every fifth day, there is great potential to monitor sub-annual processes.

Besides providing global canopy top height estimates improving beyond the state of the art, our VSM models full vertical profiles that are sensitive to small local structure variations that are not represented in canopy top height products. We show that the VSM and especially lower relative height metrics (e.g., RH25) capture such local variations including natural patterns like small canopy gaps and differences in canopy closure, but also anthropogenic disturbances like narrow forest tracks and early signs of logging and deforestation activities. Such detailed local structures are neither visible in the original sparse GEDI data, as high-spatial resolution is required, nor are they visible in canopy top height products derived from GEDI as the 25 m footprint of the laser beam leads to blurring effects[8].

Quantifying the uncertainty in estimated biophysical quantities is key to inform downstream analyses. Therefore we used conformal prediction to calibrate our estimated prediction intervals. We found that calibrating uncertainties at the biome level improves the regional coverage, that is, the probability that the true structure metric falls within the predicted interval, while only slightly increasing the prediction intervals. Ultimately, we demonstrate the benefit of using the presented VSM data for identifying pristine natural forests and find that the vertical structure data with local spatial context substantially improves the separation of natural and managed forests (by 42%), as opposed to using canopy top height data. This marks a substantial improvement for a challenging but essential task to implement deforestation policies such as EUDR.

2 Results

2.1 Modeling the full vertical structure

GEDI measures vertical vegetation structure within approximately 25 m footprints using full-waveform LiDAR. Its relative height (RH) profile provides a compact representation of the raw waveform, from which the vertical distribution can be approximately reconstructed (Fig. 1). Here we present a vertical structure model (VSM) that compensates for the sparse spatial sampling of these GEDI RH profiles by predicting the full RH profile continuously at 10 m resolution, thereby complementing GEDI's vertical information with the spatial context needed to characterize three-dimensional structural complexity caused by fine-scale climatic, geographic, and disturbance gradients[5].

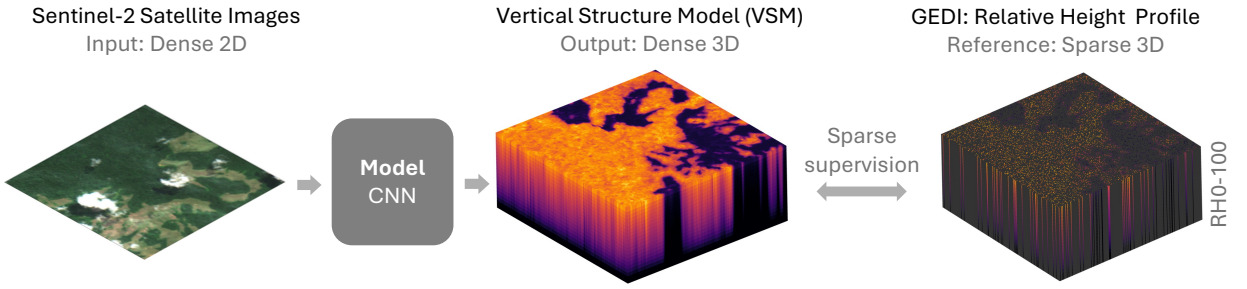


Figure 2: To densify these sparse GEDI measurements, a deep learning model computes a dense vertical structure model (VSM) from optical satellite images under sparse supervision.

Deep learning approach. To compute a global VSM, we developed a fully convolutional neural network (CNN) that combines dense 2D satellite imagery from Sentinel-2 with sparse 3D relative height (RH) profiles from GEDI to derive a dense 3D structural profile of the Earth's vegetation at 10 m resolution (Fig. 2). We build our model architecture based on prior work by Lang et al.[8] but train the CNN with a multitask strategy that jointly optimizes a quantile regression loss for each RH metric in the profile together with a cross-entropy loss for land cover segmentation. The

latter helps the model to learn robust features where GEDI reference data are scarce or unreliable. Such gaps arise from GEDI's sparse coverage and sensitivity. A strict quality filter selects 178 million measurements with good sensitivity for the training of the model. We also filter measurements on steep terrain, where the large laser footprint broadens the waveform responses and biases RH metrics as proxies for vegetation height above ground[33, 34].

To estimate vertical structure at global scale (Fig. 3) robustly under clouds and illumination variation, we adopted the late-aggregation approach from[8]. For each location, multiple growing-season images are processed independently, and the resulting VSM predictions are aggregated by their pixel-wise median. While it is challenging to visualize this full-3D VSM data cube, we can visualize the vertical profiles along local transects, e.g., the 8km long example from Northern Sumatra, Indonesia in Fig. 4 shows the transition from managed landscapes (on the left) to natural forests (on the right).

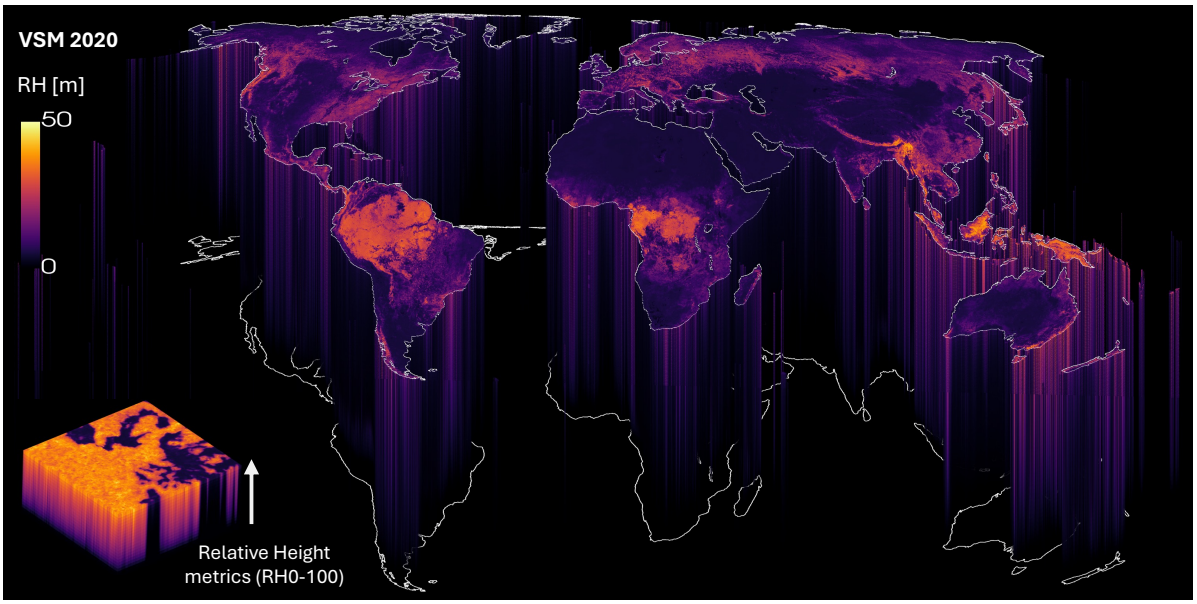


Figure 3: The global VSM for 2020. In this data cube, each 10 m pixel represents the full RH profile (RH0-RH100), characterizing vertical and horizontal vegetation structure across the Earth's land surface.

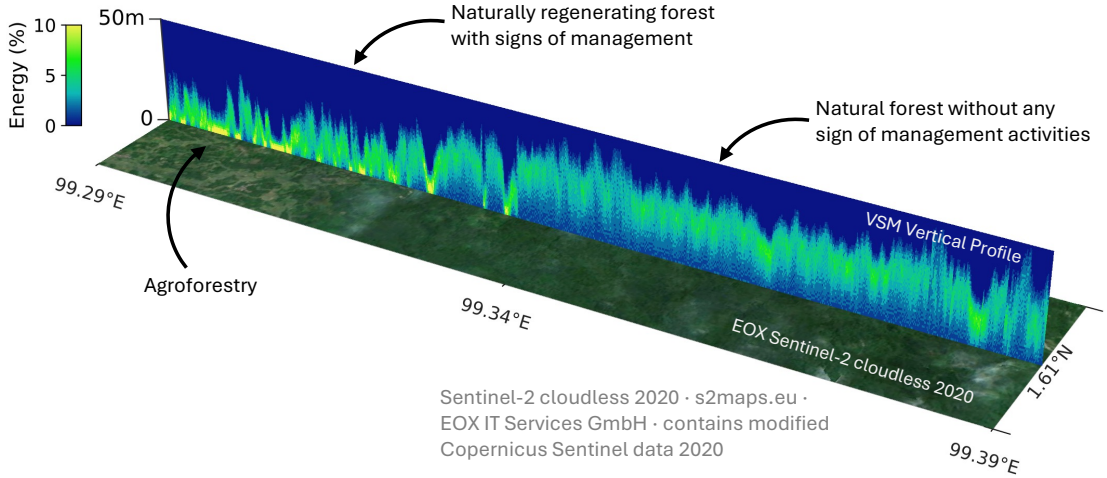


Figure 4: Example transect from Northern Sumatra, Indonesia, showing the variation of the computed 3D vertical profile as returned energy across land use types[35], from agroforestry and managed forests to natural forests. Sentinel-2 cloudless 2020: https://s2maps.eu, EOX IT Services GmbH; contains modified Copernicus Sentinel data 2020.

Conformalizing the prediction uncertainty. The reporting of modelled Earth observation data for environmentally and socially relevant tasks requires rigorous uncertainty quantification. In addition to estimating the vegetation structure (median), we use quantile regression to estimate the 5th and 95th percentile of each predicted RH metric of the full vertical structure profile. This leads to prediction intervals for every RH metric in the vertical profile at each location (Fig. 5). To get coverage guarantees, we apply split conformal prediction (SCP)[36–38], recalibrating the predicted intervals post hoc (see Methods). When evaluated globally, this calibration process results in conservative empirical coverage above the nominal 90% across all RH metrics (Fig. 6). However, the importance of calibration becomes evident when the data are stratified by biome. The uncalibrated empirical coverage falls considerably below the target of 90% for Temperate broadleaf forests across all RH metrics, while Temperate grasslands show both overcoverage and undercoverage depending on the RH level. To obtain good (conditional) coverage for each biome, we group the calibration data by WWF terrestrial biomes[39] and apply SCP independently within each biome[38]. Conformal calibration successfully brings the empirical coverages closer to the target 90% across all 13 calibrated biomes and all RH metrics on the held-out test data (Fig. 6). This is a substantial improvement over using the uncalibrated quantiles.

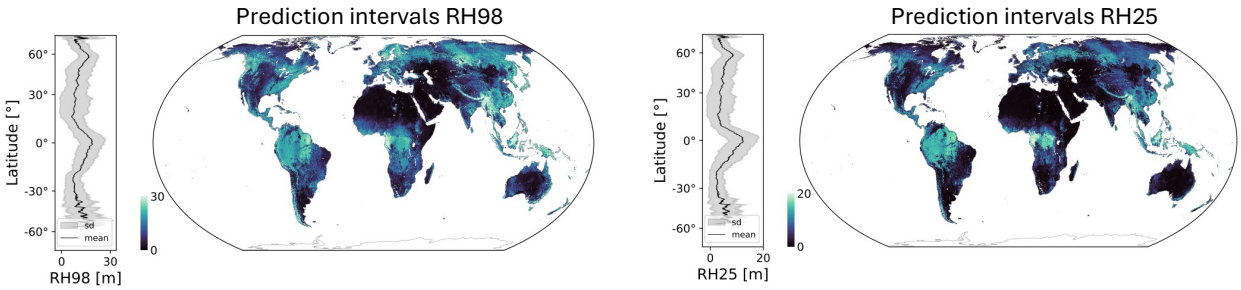


Figure 5: Global distribution of prediction intervals for RH98 (left) and RH25 (right), with corresponding latitudinal distributions.

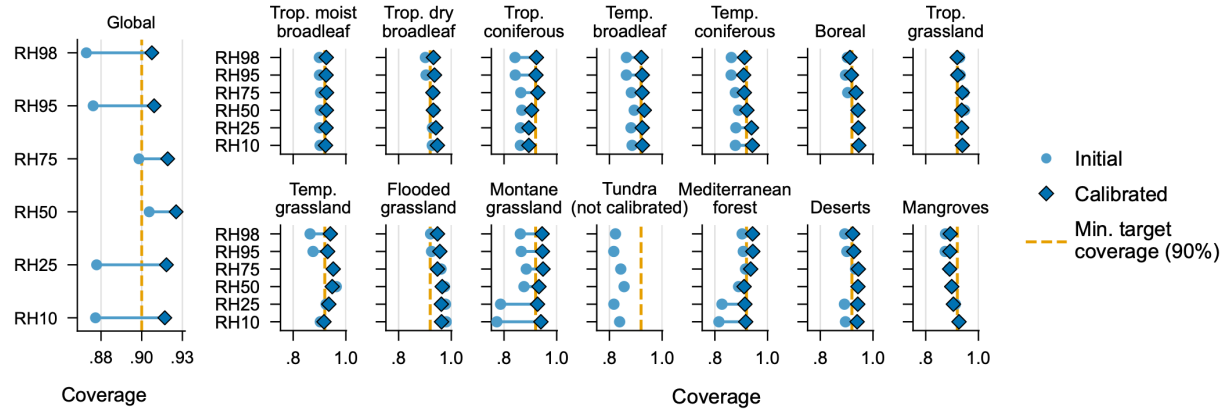


Figure 6: Coverage of prediction intervals improves after calibration with conformal prediction, evaluated globally (left) and stratified by biomes (right).

The VSM reproduces vertical structure and its diversity. Validation against held-out GEDI shows that our VSM reproduces the GEDI RH profile well, with residuals centered near zero across all RH bins (Fig. 7). Agreement is closest in the mid-canopy, with larger deviations toward the lower and upper ends of the profile. At the lower end (RH0–19), the predicted distribution is concentrated more narrowly around the mean, reflecting the difficulty of inferring lower-canopy and sub-canopy-related RH metrics from optical imagery alone. At the upper end (RH90–100), the VSM better represents the variance observed by GEDI, but still underestimates variation.

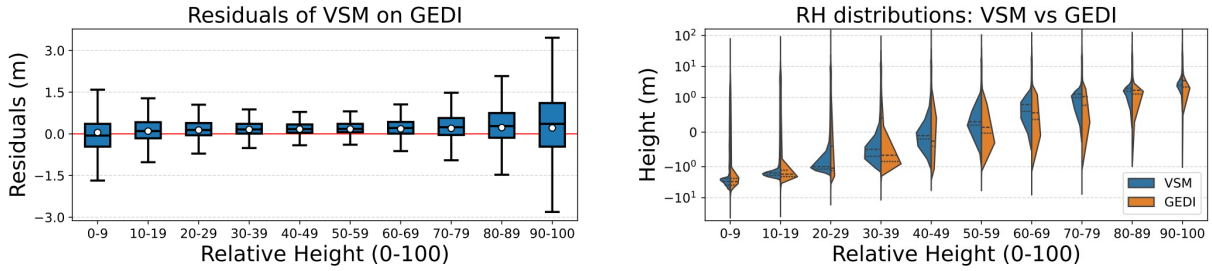


Figure 7: Error distribution (left) and absolute distribution (right) of the estimated RH metrics compared to hold-out GEDI reference data.

VSM-derived structural diversity indices also agree well with those computed from the GEDI reference (Fig. 8), showing its ability to preserve higher-order structural properties. We consider four indices that capture different aspects of vertical canopy complexity and have been widely used in biodiversity and habitat assessments[40, 41]: foliage height diversity (FHD)[40], one- and two-dimensional effective number of layers (1D and 2D ENL)[42], and canopy ratio (CR)[43]. Agreement is strongest for FHD ($R^2 = 0.80$) and lowest for CR ($R^2 = 0.59$). This is consistent with the narrower VSM distribution observed at lower RH metrics (Fig. 7), as CR is sensitive to errors in the understory structure estimates.

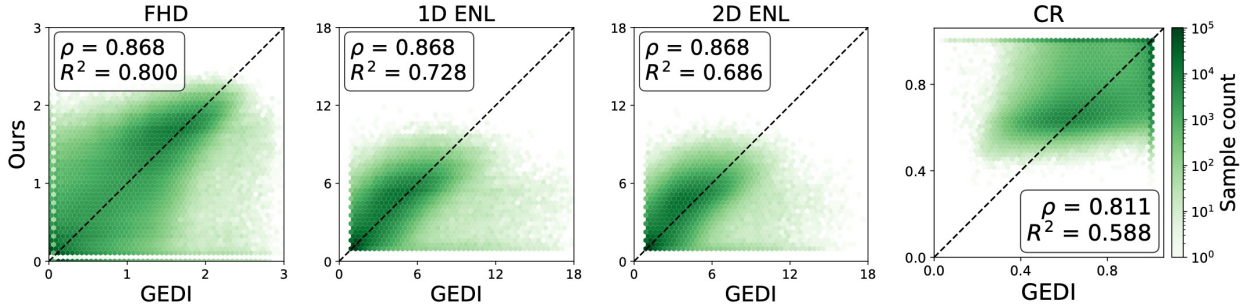


Figure 8: Agreement between diversity indices derived from the VSM and GEDI, at the footprint level.

Comparison against the Waveform Structural Complexity Index (WSCI)[5] further confirms that the VSM captures 3D structural complexity, with all four VSM-derived indices showing strong agreement with WSCI (Fig. 9). Based on the GEDI RH metrics, the WSCI models a 3D canopy entropy metric derived from globally distributed airborne laser scanning (ALS) training data. Agreement is strongest in the mid-range of WSCI. At lower WSCI values, the diversity indices concentrate near their theoretical lower bounds (upper bounds for CR). At higher values, where WSCI saturates around 11, VSM-derived indices continue to vary, showing its ability to capture broad gradients in 3D structural complexity.

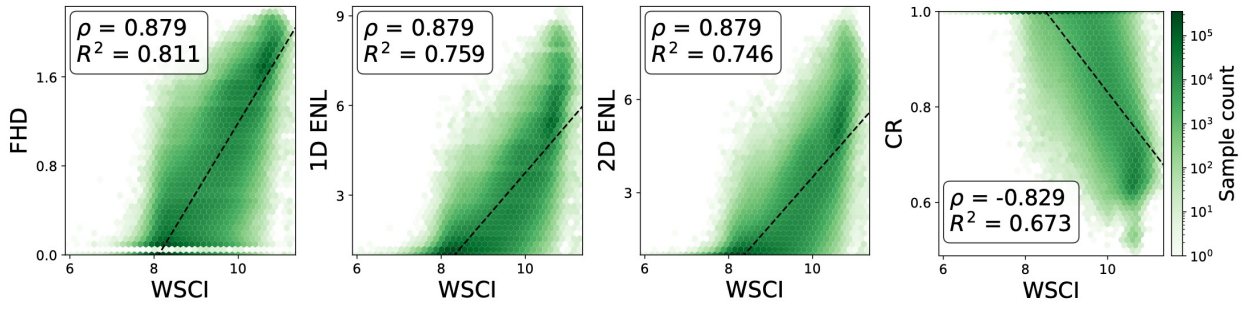


Figure 9: Agreement between VSM-derived diversity indices and the Waveform Structural Complexity Index (WSCI)[5] at 1 km resolution.

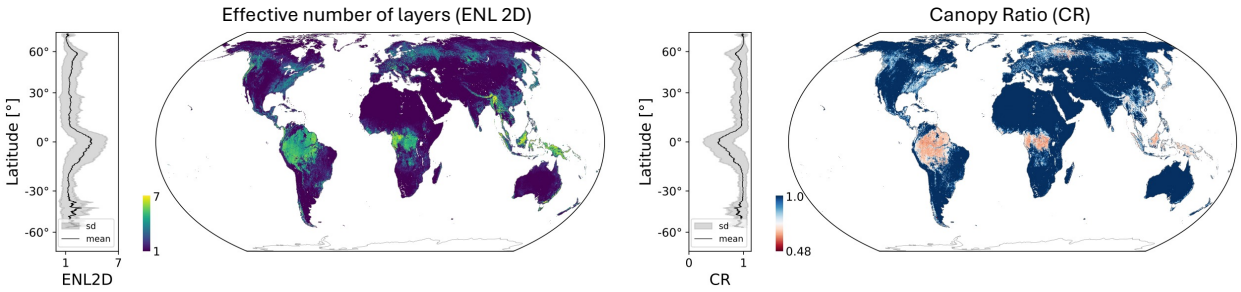


Figure 10: Global distribution of the VSM-derived diversity indices 2D effective number of layers (ENL) and canopy ratio (CR) at 1 km, with corresponding latitudinal profiles.

The evaluation of our canopy top height (RH98) estimates with independent airborne LiDAR data from diverse geographic regions and different years showed good overall agreement, with average Spearman's rank correlation coefficient of $\rho = 0.71$ and $\rho = 0.77$ for the two airborne instruments (Extended Data Fig. A2). Because RH-profile definitions are not standardized across airborne LiDAR datasets, we used canopy top height as a general cross-site quality check for our VSM, as it can be more readily harmonized across datasets. Across sites with diverse vegetation characteristics the ρ ranged from 0.53 (tropical moist broadleaf forests and savanna, Gabon) to 0.89 (mangroves and tropical moist broadleaf forests, Gabon).

Together, these evaluations establish the VSM as a reliable representation of vertical structure and its diversity, supporting the global analyses that follow, with limitations concentrated in the understory and dense canopy tops.

Global patterns of vertical structure and uncertainty. Our global VSM allows to derive established structure indices describing vertical structure traits, including FHD, 1D and 2D ENL, and CR, at 10 m spatial resolution globally. Looking at the global distribution of ENL 2D and CR at 1km resolution (Fig. 10) we see a clear latitudinal gradient with higher number of effective layers in the tropics which is decreasing towards north and south. Similar latitudinal patterns are observed for the CR, which is lowest in the tropics and increases towards higher latitudes. The CR is computed as $CR = (\text{RH98} - \text{RH25})/\text{RH98}$ and complements ENL as an indicator of the asymmetry of vertical structure distribution. A CR value of 0.74 indicates a rather symmetrical distribution, while a CR lower than 0.74 indicates that vegetation structure is denser in the upper layer and vice versa[44].

Hotspots of ENL are found in tropical forests such as Gabon, central Borneo, and north-eastern Amazonas but also in northern Myanmar, which is in agreement with prior global structural complexity studies[5]. While for Gabon and central Borneo, the CR decreases with distance from the forest boundary, for northern Myanmar the CR is more homogeneous and around 0.74. This indicates rather uniform distribution of the estimated vertical profile and vegetation with less canopy closure (see, e.g., Fig. 11). Such latitudinal gradients are also reflected in our prediction intervals (Fig. 5). On a global scale, uncertainty correlates with the top height and vertical structure, following similar latitudinal gradients like ENL (Fig. 10). However, at local scales, we find that estimates with similar RH values can have varying prediction interval widths (see Extended Data Fig. A3).

2.2 Forest naturalness quantification benefits from vertical structure

Our results on forest naturalness classification show that vertical structure is a strong predictor of forest naturalness. Incorporating the full VSM profile together with its spatial context improves accuracy relative to the canopy top height baseline for all classes, with the largest gains (up to 0.65 in F1 score) for plantation types that are indistinguishable by top height alone. These differences are highly statistically significant (paired two-sided Wilcoxon test, $p \ll 0.001$).

Distinguishing natural forests from managed forests and plantations is a prerequisite for effective conservation planning[24] and EUDR implementation. However, quantifying forest naturalness from remote sensing data remains challenging [45], especially when forests have similar canopy height and cover but differ in their internal layering. Natural forests typically develop multi-layered canopies with high structural complexity, whereas planted and intensively managed forests tend to exhibit uniform, single-layered profiles[46]. These differences extend below the canopy top and influence both ecosystem integrity and function [24, 47], with lower and middle canopy layers contributing strongly to 3D forest structural complexity, particularly for tropical forest[5]. Qualitatively, the VSM shows clear distinctions across different forest disturbance and recovery states (See Fig. 12). To evaluate whether our VSM encodes sub-canopy features informative of forest naturalness, we classify expert-annotated forest management classes[35] starting with top height (RH98) and progressively adding vertical-structure information.

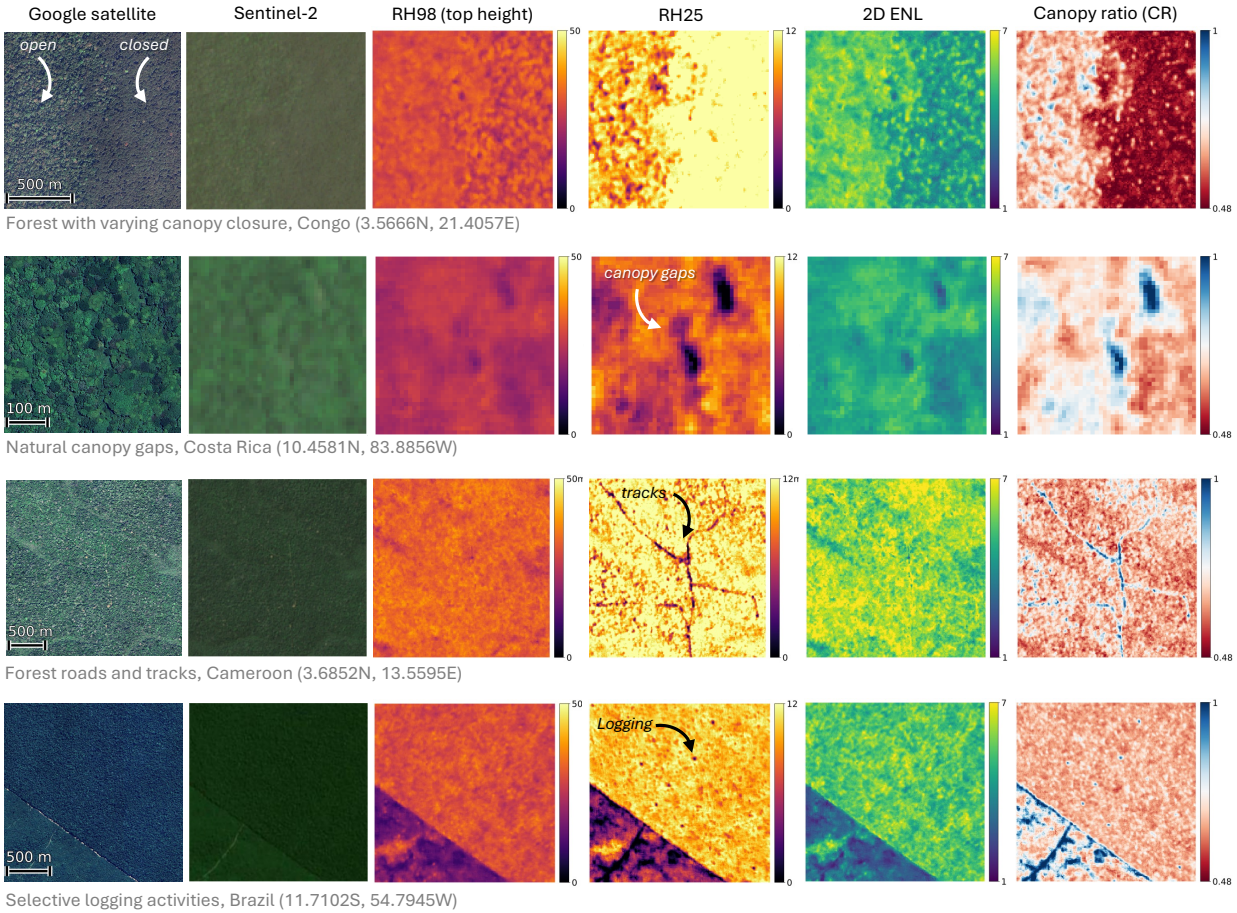


Figure 11: Four tropical forest sites showing how the VSM captures fine-scale structural variations. From top to bottom: forest with varying canopy closure, natural canopy gaps, narrow forest roads and tracks, and selective logging.

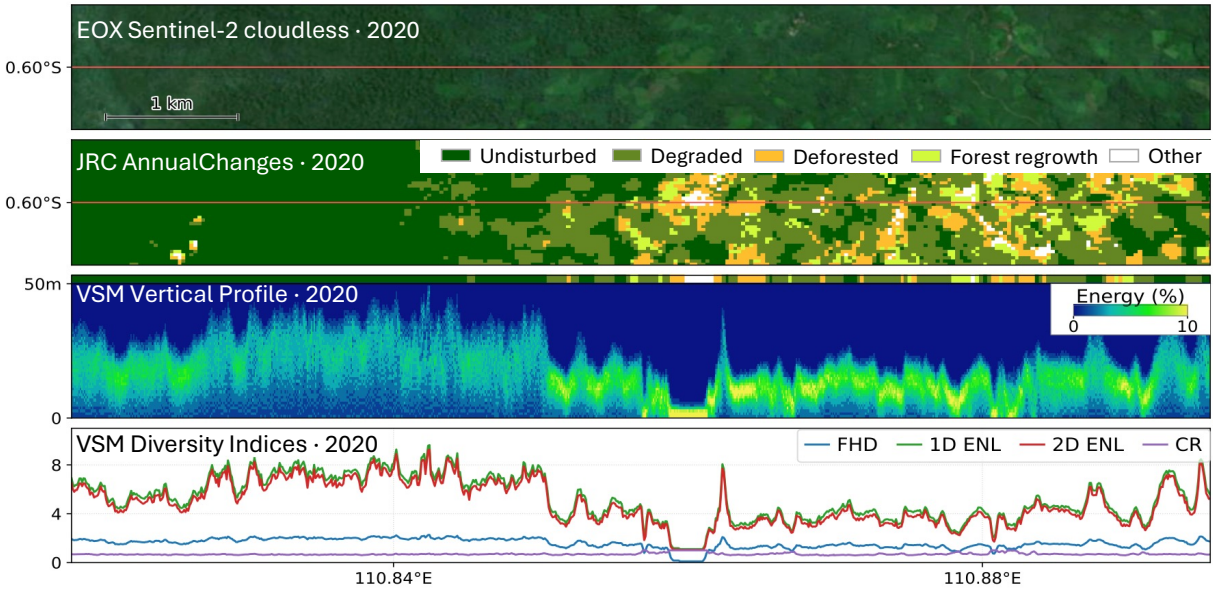


Figure 12: Example transect from Borneo, Indonesia, illustrating how vertical structure varies across disturbance regimes. Sentinel-2 cloudless 2020: https://s2maps.eu, EOX IT Services GmbH; contains modified Copernicus Sentinel data 2020. Forest disturbance classes from JRC TMF AnnualChanges v1 [48] are shown for visual reference.



Figure 13: **VSM improves forest naturalness classification. a,** We show the importance of the spatial context provided by the VSM for classifying forest naturalness using a linear model (logistic regression). Higher F1 scores are better, and hatched bars show the improvement from incorporating spatial context. **b,** Contribution of vertical structure data for classifying forest naturalness using a non-linear model (convolutional neural network). Hatched bars show the improvement over using canopy top height (RH98) as the predictor. We compare commonly used diversity indices (FHD, ENL, CR) with key RH metrics and the full profile from the VSM and its complementarity with Sentinel-2 images (S2).

First, we show that the local variation of the VSM provides complementary spatial context that is not captured by sparse GEDI footprint locations. Using logistic regression (Fig. 13a), the spatial context improves the overall F1 by 19% yielding consistent gains across all landcover categories with the largest gains in managed classes such as planted forests, plantations, and oil palm. This confirms that the spatial variation is particularly informative for classes with characteristic spatial signatures, such as the regular planting patterns, but also informative for natural forest patterns, which point-wise sampling cannot capture.

Second, full vertical profile information improves forest naturalness classification beyond what canopy top height provides by 42% in F1. Using a CNN classifier (Fig. 13b), the overall F1 score increases progressively with richer vertical structure information. Substantial improvements are observed for planted forest, short rotation plantation and oil palm, which cannot be distinguished from top height (RH98) alone. Planted forest remains the hardest class, where adding a single vertical complexity measure to canopy top height (RH98) is insufficient, and substantial improvement requires the full profile.

Finally, we show that adding spectral data from Sentinel-2 is complementary and can improve classification performance when combined with both, RH98 and the full profile. Combining the full profile with Sentinel-2 achieves the best performance across all naturalness classes, with the largest gain on the most challenging type, planted forest, indicating that the full profile and Sentinel-2 imagery contain complementary information. Interestingly, combining multiple structural diversity indices does not outperform the combination of few key RH metrics, suggesting that key RH metrics

Table 1: Comparison of the VSM with existing canopy top height products, where each product is evaluated against its corresponding RH proxy metric. All canopy height products are resampled to 10 m for consistent comparison. All differences between our VSM and the other models are highly statistically significant (paired two-sided Wilcoxon test, $p \ll 0.001$).

	RMSE			MAE			ME (bias)		
	RH95	RH98	RH100	RH95	RH98	RH100	RH95	RH98	RH100
UMD	5.59			3.77			-1.97		
ETH		6.03			4.31			-0.23	
UM			5.33			2.76			-1.45
META	6.42			4.21			-3.54		
Ours	**4.68**	**4.87**	**5.02**	**2.43**	**2.61**	2.79	**0.22**	**0.20**	**0.13**

contain more complementary information than the commonly used structural diversity indices. A similar pattern holds for logistic regression (Extended Data Fig. A4).

Together, these results show that our VSM captures 3D structural information beyond canopy top height and sparse GEDI locations and supports applications in which assessing vertical and spatial heterogeneity is crucial.

2.3 Advancing global canopy top height estimates

Our VSM yields state-of-the-art global canopy top height estimates, with particularly robust performance in tropical and frequently cloudy regions. Canopy top height has been identified as a priority biodiversity metric to observe from space[49]. Although most existing global canopy top height products utilize GEDI data as the reference, they use different RH metrics as proxies for canopy top height (i.e., RH95, RH98, and RH100). These differing definitions of top height hinder proper comparison between the products, as height increases with higher RH metrics. Our VSM provides all RH metrics and allows us to use top height estimation as a familiar benchmark. We present the first fair comparison against state-of-the-art top height products (Table 1), henceforth referred to as UMD[7], ETH[8], UM[9], META[50]. Our VSM advances the state of the art of top height estimates globally for the year 2020. Compared to the commonly used META canopy height map max-pooled to 10 m resolution, our estimates improved by 37% in root mean square error (RMSE). Closest to our performance is the UM map, however, it is based on RH100, which is prone to atmospheric noise[4].

Qualitatively we find that our top height maps are sharper than the ETH map and comparable with UM, likely because the UM map and our VSM were trained on the GEDI version 2 reference data, which provides an improved footprint geolocation compared with version 1 used by ETH. We find that our product substantially outperforms other products in tropical and frequently cloudy regions (see Extended Data Fig. A5 column A-D). While our canopy top height proxies have a lower overall bias than prior work, they still underestimate very tall canopies (like all prior work), which is likely an effect of the signal saturation in Sentinel-2 imagery. Unlike[8], we do not apply any re-weighted loss to improve performance on rare tall canopies, as this typically comes at a price of overestimating lower canopies.

2.4 Modeling structure beyond top height resolves small-scale patterns

While our VSM advances the state of the art in canopy top height estimation, top height alone remains an incomplete descriptor of vegetation structure, as illustrated in the forest naturalness analyses, where adding the full profile and its spatial context markedly improved classification over a canopy top height baseline. In the following, we show that GEDI-derived top height data is equally blind to small-scale structure. While the modelled top height proxies, such as RH98, tend to close canopy gaps smaller than the GEDI footprint, we show for the first time that the lower RH metrics, e.g. RH25, are sensitive enough to resolve such fine-scale structures.

Across four tropical sites, lower RH metrics and some VSM-derived diversity indices reveal fine-scale features that top height (RH98) does not capture (Fig. 11). In Congo, the variation in canopy closure is well represented in the CR map, while the 2D ENL reflects the high spatial variance in open canopy. In Costa Rica, small natural canopy gaps that RH98 tends to close remain clearly visible in RH25. In Cameroon, RH25 and CR resolve narrow forest tracks that RH98 misses and are nearly invisible in the Sentinel-2 image. Lastly, in Brazil, RH25 and CR expose selective logging, where individual missing trees along an access track are clearly identifiable. Although such logging activities are nearly impossible to see with the naked eye, neither in very high-resolution satellite images nor in Sentinel-2 images, our

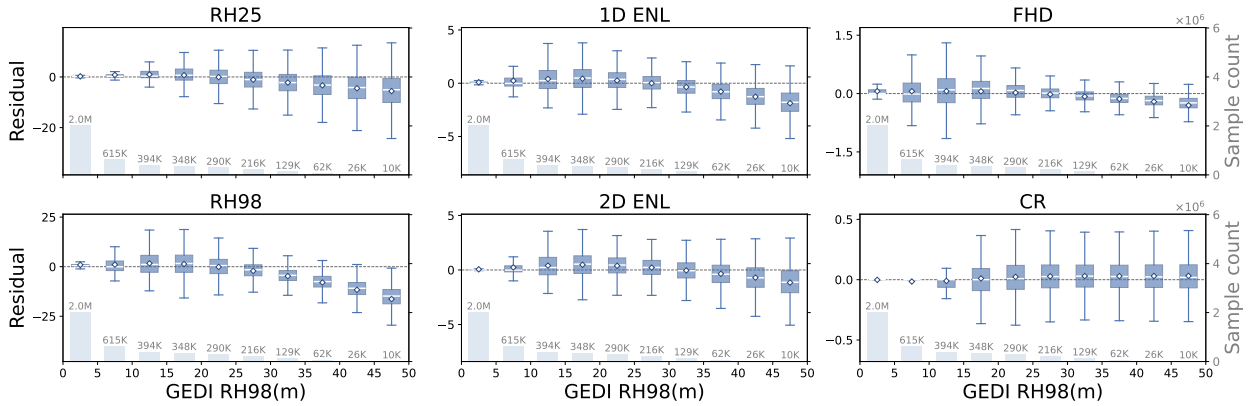


Figure 14: Error distributions of vertical structure metrics with respect to canopy top height intervals (RH98), at the footprint level. Bars indicate sample counts per bin on the right vertical axis.

model has learned to be sensitive to predictive texture patterns in Sentinel-2. The logging area is recorded by SIMEX (System for Monitoring Timber Harvesting) in the Brazilian Amazon[51].

Collectively, GEDI top-height proxies such as RH98 are not sensitive to small canopy structures. Even when modeled at 10 m spatial resolution, top height maps tend to close canopy gaps smaller than the GEDI footprint of 25 m diameter as the highest vegetation within the footprint dominates these measurements. However, when modeling lower RH metrics, such as RH25, the resulting maps retain sensitivity to those sub-footprint structures, which yields complementary information that is, e.g., useful for quantifying forest naturalness and forest disturbances at fine scale. Consequently, these local structures are well represented in those diversity indices that make use of the full profile or the lower RH metrics such as the CR.

3 Discussion

3.1 Limitations

This study presents a global high-resolution vertical structure models (VSM) at 10 m spatial resolution. While we demonstrated that the computed data product is predictive of forest naturalness and sensitive to represent fine-scale structural signatures, some limitations exist. The underestimation of canopy top height for tall vegetation is a common challenge due to the limited sensitivity of optical reflectance to top height variations in tall and dense forest[8]. We observed that the errors of the VSM-derived diversity indices also vary with top height (Fig. 14). This is likely a result of the reduced sensitivity to capturing spatial patterns in the optical satellite imagery as vegetation density and canopy closure increases. All indices, except the canopy ratio, follow a similar trend where their underestimation increases with vegetation height above 25–30 m. Canopy ratio does not show this bias, even for tall canopies; here a different multiplicative scaling of the RH values from a different source cancels out. Consequently, our VSM should be interpreted as a conservative estimate of structural complexity. Our provided prediction intervals further inform downstream applications about the expected data quality (Fig. 5).

These systematic differences need to be accounted for when using the VSM for any downstream task. To reduce error propagation, it is best practice to recalibrate models on VSM-derived data instead of applying algorithms or formulas tuned for the original GEDI data. However, as we have demonstrated for the task of forest naturalness quantification, this is not necessary when models are directly calibrated using the VSM as predictor data.

Our VSM is further influenced by GEDI's own measurement limitations. Uncertainty in footprint geolocation adds noise and in dense canopies most laser energy is reflected by the upper layers, leaving the waveform less sensitive to the understory[4]. As a large-footprint laser, its ground measurements are also affected by steep-terrain. We addressed these issues by using several quality filters, trading training data quantity for quality. GEDI's global coverage is also confined to $\pm 51.6^\circ$ latitude north and south. As a result, the prediction reliability varies across regions, since the training distribution does not necessarily match all deployment conditions, an issue we partially address through per-biome conformal calibration[38] of the prediction intervals. Our independent evaluation with high-quality airborne LiDAR data from several regions shows that the agreement is good in both areas outside the GEDI coverage and in mountainous terrains. This strong generalization of our approach is likely a result of training a global model on more than 178 million data points and our multitask strategy, which makes the learning robust in regions where GEDI data is scarce.

To obtain a complete data layer in regions of frequent cloud cover, we aggregate predictions from multiple image observations to create annual estimates. These composites may contain artifacts due to imperfections in the cloud masks and fast landcover changes that lead to mixed signals. To better study such scenarios, e.g. deforestation or damage after hurricanes, our model could be applied to single cloud-free satellite images to create a clear time series of structural changes.

Finally, dense canopies remain challenging to model because optical satellite imaging sensors cannot "see through" closed canopies. Our model instead learns statistical correlations between spectral and textural patterns in the image and vertical structure profiles conditioned on geolocation. The future combination with complementary data from active imaging sensors, like the ESA BIOMASS mission[52], seems a promising research direction. Nevertheless, our VSM captures vertical structure within the 25 m GEDI footprint, which is sensitive to small canopy gaps and variation in canopy closure. Such patterns are not necessarily visible by the human eye, but a predictive signal for our model that learned to estimate the vertical structure measured by GEDI.

3.2 Facilitating scientific advancements

Many environmental modeling applications require the ability to *pair geographically sparse data points* with vertical structure data, for example, carbon flux measurements, biodiversity observations, and aboveground biomass field data. Having access to a dense VSM facilitates data pairing substantially. Our approach complements efforts on mapping global vegetation properties[50, 53, 54] by improving the spatial resolution and coverage of global vertical structure data.

Improving natural forest maps will be a key application of our global VSM data. Our case study has already shown the benefit of natural forest classification and its sensitivity to different forest management categories. Deploying a forest naturalness classifier is technically feasible and could complement ongoing mapping initiatives[55] to support the implementation of forest degradation and deforestation policies. *Management of forest resources* at local scales is directly supported by the new VSM data, as it is sensitive to human activities such as logging. Not only is this relevant for countries that lack access to high quality airborne LiDAR data, but even in Europe, where high quality airborne data is often part of national monitoring strategies, the revisit time of ALS campaigns is often in the order of 5 years, preventing timely monitoring. Our approach allows to compute annual, or even monthly VSMs, as in principle only a single cloud-free Sentinel-2 image is needed to make a prediction.

Monitoring carbon stocks and biodiversity are urgent challenges where remote sensing data offers a key technology[26, 56]. Our provided VSM has the potential to improve these applications. While our VSM comes at 10 m resolution, the spatial resolution of derived aboveground forest biomass estimates should be adapted to the natural resolution constraints and the reference field plot data[57]. This does not preclude the use of high resolution predictors, which can better capture fine-scale spatial variability and thereby improve biomass estimates at coarser output resolution. *Habitat characterization* will benefit from the sensitivity to small natural canopy gaps and varying canopy closures describing heterogeneity beyond the sensitivity of existing products. These are important characteristics for modeling light availability and below-canopy temperatures, crucial drivers of forest biodiversity as well as ecosystem dynamics and resilience. This sensitivity will also advance *early warning systems* since our approach can support both the detection of deforestation and forest degradation activities, which has been reported to account for more than half of all biomass loss in tropical forest[58]. Early signs of human activities, such as narrow forest tracks and even selective logging, are often small in spatial extent and challenging to detect with remote sensing data, but become detectable in our data.

While our experimental findings indicate that the presented VSM at 10 m spatial resolution advances the characterization of natural and managed forests, as well as the detection of small-scale structures, future collection of both airborne and spaceborne LiDAR data would reduce the remaining uncertainty of the global vegetation structure distribution. Nevertheless, our approach estimates the distribution for the year 2020 and enables both the estimation of the current status and going further back in time, based on historical archives of optical satellite remote sensing data. This data, therefore, has great potential to contribute to a broad range of timely scientific advancements in understanding the global distribution and dynamics of carbon stocks and biodiversity in the wake of global environmental change.

4 Methods

4.1 Data

GEDI L2A Relative Height. NASA's Global Ecosystem Dynamics Investigation (GEDI) is a full-waveform LiDAR instrument that provides sparse observations of forest vertical structure within approximately 25 m footprints with near-global coverage. We use the Level-2A product, which summarizes each waveform as 101 relative height (RH)

metrics (RH0–RH100). Each RH metric measures the height above ground below which a given percent of the cumulative waveform energy has been returned, for example, RH98 refers to the height at which 98% of the LiDAR waveform energy is returned. Together, these 101 RH values describe the vertical distribution of vegetation and are used as a proxy for the vertical vegetation structure. The RH metrics provide a fixed-length representation of the raw waveform, embedding it into $\mathbb{R}^{101}$, which makes them well-suited for predictive modeling.

We originally sampled 300 million high-quality, leaf-on GEDI footprints from 2019–2022 using a spatially uniform sampling across global landmass. Because deciduous vegetation exhibits strong seasonal variation in canopy structure, we restricted the training data to leaf-on conditions. To select representative footprints for the vertical vegetation structure, we remove low-sensitivity observations following[5], which are unreliable measurements with insufficient laser energy to detect the ground return beneath dense canopies. After sensitivity filtering for representative points for the vertical vegetation structure, we ended up with 178,963,797 points. Following[8], we applied standard GEDI quality filters as listed in Table A1 in Appendix A. The GEDI instrument is integrated into the International Space Station (ISS), which follows an inclined orbit resulting in a disproportional high observation density near 51° N. Due to this latitudinal bias, a simple uniform sampling of GEDI orbits fails to produce a representative global distribution across terrestrial landmasses. To mitigate this spatial oversampling and ensure geographic uniformity, we partitioned the GEDI footprints into Military Grid Reference System (MGRS) cells and allocated samples proportionally to the land area of each cell, scaled by a fixed sampling density (samples per km^2). The data were downloaded from Google Earth Engine (GEE).

Sentinel-2 Level-2A. We use Sentinel-2 multispectral imagery as the primary input for our model. Prior work has demonstrated that canopy top height can be derived from optical imagery alone[7, 8, 50, 59]. Here, we investigate whether optical imagery can provide enough information to predict the vertical vegetation structure beyond canopy top height. Sentinel-2 provides global imagery in 13 spectral bands at 10–60 m resolution and a revisit time of approximately five days, making it well suited for large-scale vegetation structure modeling. In this work, we use the 12 spectral bands (all bands except the cirrus band) as inputs.

To construct the training dataset, Sentinel-2 observations are matched to individual GEDI footprints. For each GEDI footprint, we apply a two-stage filtering procedure to ensure high image quality. Candidate scenes are first filtered at the scene level by removing scenes with cloud cover $\geq 50\%$ or water coverage $\geq 99\%$. The permissive water threshold retains scenes covering coastal areas and small islands, where most of a scene may be ocean despite containing valid GEDI footprints over land.

We then constrain the temporal search window based on vegetation type. For deciduous forest, we restrict the candidate scenes to the leaf-on period with the time window defined by the GEDI footprint attributes *leaf_on_day* and *leaf_off_day*. When *leaf_on_day* exceeds *leaf_off_day*, indicating a growing season that spans the calendar-year boundary, we add 365 to *leaf_off_day* so that the search window can extend into the following year. For evergreen forest and non-vegetated land-cover classes, where seasonal leaf-on and leaf-off dates are not defined, we select scenes acquired within a $\pm$90-day window of the GEDI acquisition date. This filtering is performed for each individual GEDI footprint independently. Consequently, geographically adjacent GEDI footprints may be assigned different candidate scenes because of differences in acquisition dates and local growing-season timing. In the second stage, we filter at the patch level. We follow[8] and extract a 15×15 pixel patch centered on each GEDI footprint, which showed that a 15×15 patch provides sufficient local context for canopy height prediction. For each patch, we compute the fraction of defective pixels using the Sentinel-2 Scene Classification Layer (SCL). Pixels flagged as no-data, saturated or defective, medium- and high-probability clouds, cirrus, snow, or ice are classified as defective. Patches with a defective pixel fraction exceeding 0.2 are excluded. The remaining candidate patches are ranked first by the number of valid pixels and second by temporal proximity to the GEDI acquisition date. The highest-ranked patch is retained.

ESA WorldCover. To provide additional spatially dense supervision, we introduce an auxiliary land-cover classification task using the ESA WorldCover product. ESA WorldCover provides global land cover maps for 2020 and 2021 at 10 m resolution, derived from Sentinel-1 radar and Sentinel-2 optical imagery. The maps distinguish 11 classes defined using the Land Cover Classification System (LCCS) developed by the United Nations Food and Agriculture Organization (FAO). For each GEDI footprint, we extract the corresponding ESA WorldCover 2021 (v2) patch. Although our GEDI data span 2019–2022, we assume that the majority of pixels retain the same land-cover class over this period. This auxiliary task serves three purposes. During training, it provides dense spatial supervision and encourages the model to learn spatially continuous features that cannot be inferred from the sparse and irregularly distributed GEDI footprints alone. At inference, the predicted land cover map can be used to mask non-vegetated areas during post-processing, removing the need for an external land-cover product in years when ESA WorldCover is unavailable. Additionally, the predicted land-cover classes can improve interpretability by linking the model's internal representations to ecologically meaningful categories.

Slope derived from Copernicus DEM. Terrain slope is a well-documented source of error in GEDI canopy height estimates. On steep slopes, the ground return in the GEDI waveform broadens as the ground surface spans a range of elevations within the 25 m footprint, leading to mixing of ground and canopy signals and systematic overestimation of canopy height[33, 34]. This effect becomes pronounced on slopes exceeding approximately 15°, where canopy height estimates show a positive bias and increased error[60]. Furthermore, GEDI's horizontal geolocation uncertainty ($\approx$10 m) translates into larger vertical errors on steep terrain, further increasing uncertainty in vegetation height estimates[61]. To mitigate these effects, we exclude GEDI footprints where the terrain slope exceeds 20°, following[9]. Slope is derived from the Copernicus DEM GLO-30, a global digital elevation model at 30 m resolution based on the TanDEM-X mission[62]. We compute slope from the DEM and resample it to 10 m resolution using bilinear interpolation to match the spatial grid of the Sentinel-2 imagery and ESA WorldCover product. The resulting slope layer is used to identify and mask GEDI regression targets located on steep terrain ($> 20°$), where vegetation height estimates are known to be less reliable.

Data sets. Combining the data sources described above yielded approximately 178 million samples spanning 13,929 Sentinel-2 tiles between 2019–2022. To avoid overly optimistic performance estimates arising from spatial autocorrelation, we partition the data geographically at the Sentinel-2 tile level rather than at the sample level. In addition to the standard training, validation, and test sets, we reserved a separate calibration set for uncertainty calibration via split conformal prediction (SCP)[36–38]. The geographic partition assigns 70% of tiles to training, 10% to validation, 10% to calibration, and 10% to testing, corresponding to 114,403,775 training, 20,702,174 validation, 21,251,628 calibration, and 22,606,220 test samples.

4.2 Neural network architecture

Our model builds on the fully convolutional neural network architecture of[8], which employs residual blocks with separable convolutions[63] without any downsampling. Because the network is fully convolutional, it can be applied to arbitrarily large images during inference. However, this creates a train–inference mismatch: when applied to larger patches, the receptive field exceeds the 15 $\times$ 15 pixel patches used during training, which means that the model sees more real values that were zero-padded before. To eliminate this mismatch, we redesign the network such that its receptive field exactly matches the training patch size. Specifically, we reduce the network depth to three separable convolution blocks[64]. This ensures the model operates on the same spatial context during training and inference. To compensate for the reduced depth, we double the feature width to 512 filters per block and insert a pair of 1 $\times$ 1 convolution blocks before each separable convolution block, increasing model capacity without enlarging the receptive field. Following Lang et al.[8], the model takes 12 Sentinel-2 optical bands together with cyclically encoded geographical coordinates as input, allowing the model to capture large-scale geographic variation in vegetation structure.

We adopt a quantile regression loss to train the CNN, predicting the 5th, 50th, and 95th percentiles for each RH metric independently[65, 66]. This choice is motivated by several properties of the regression task. First, the global vegetation height distribution is right-skewed, with a small number of very tall trees and occasional extreme observations. The conditional median provides a robust measure of central tendency that is less sensitive to extreme values than the conditional mean. Second, prediction uncertainty is not heteroscedastic. Structurally heterogeneous forests exhibit greater variability than homogeneous plantations, and uncertainty may also vary across different RH metrics. Quantile regression naturally captures this heteroscedasticity by allowing prediction intervals to expand or contract according to local prediction difficulty. Third, the prediction intervals produced by quantile regression are not constrained to be symmetric around the median. This flexibility is appropriate when the underlying distributions are expected to be skewed, as is typical for canopy height. For example, a symmetric $\pm$6 m interval around a predicted tree height of 5 m would imply a lower bound of -1 m, which is physically meaningless. Quantile regression can help to avoid this by allowing the lower and upper intervals to adapt independently, producing a tighter lower bound reflecting the physical constraint and wide upper bound reflecting the possibility of tall trees. However, quantile regression cannot be expected to provide calibrated prediction intervals with formal guarantees in our setting, and we use conformal prediction to address this issue (see Calibration using conformal prediction).

4.3 Training strategy

Multi-task training. Our neural network model has two heads, one for the main quantile regression task and one for the auxiliary task of classifying land cover. We perform multi-task learning, in which the loss functions for the two tasks are additively combined.

For the regression part, we use the pinball (quantile) loss[65, 66]. Given a target RH metric RH_k at level k and corresponding predicted τ-quantile $\widehat{\mathrm{RH}}_k^{(\tau)}$, the per-sample loss is

$$L_\tau\left(\widehat{\mathrm{RH}}_k^{(\tau)},\, \mathrm{RH}_k\right) = \max\big(\tau\, e,\ (\tau-1)\, e\big), \quad e = \mathrm{RH}_k - \widehat{\mathrm{RH}}_k^{(\tau)}. \tag{1}$$

The full regression loss averages over all 101 RH metrics and three quantile levels $\mathcal{T} = \{0.05,\, 0.50,\, 0.95\}$, and is given by

$$\mathcal{L}_{\mathrm{reg}} = \frac{1}{101 \times 3} \sum_{k=0}^{100} \sum_{\tau \in \mathcal{T}} L_\tau\left(\widehat{\mathrm{RH}}_k^{(\tau)},\, \mathrm{RH}_k\right). \tag{2}$$

The land cover classification loss $\mathcal{L}_{\mathrm{cls}}$ is the standard cross-entropy loss over 12 ESA WorldCover classes $\mathcal{Y}$

$$\mathcal{L}_{\mathrm{cls}} = -\sum_{c \in \mathcal{Y}} y_c \log \hat{y}_c, \tag{3}$$

where y_c is the ground-truth one-hot label for class c and $\hat{y}_c$ is the predicted probability for class c. The overall loss reads

$$\mathcal{L} = [\![s \le 20^\circ \wedge c^* \in \mathcal{Y}_{\mathrm{veg}}]\!] \cdot \mathcal{L}_{\mathrm{reg}} + \mathcal{L}_{\mathrm{cls}}, \tag{4}$$

where s is the slope, $c^* \in \mathcal{Y}$ the ground-truth class (i.e., $y_{c^*} = 1$), and $\mathcal{Y}_{\mathrm{veg}} \subset \mathcal{Y}$ the vegetation cover subset of ESA WorldCover classes at the current point, and $[\![\cdot]\!]$ denotes the Iverson bracket. Together, these conditions disable the regression loss for non-vegetated pixels and ones with slope $> 20^\circ$. The vertical profile estimates from waveform LiDAR are less reliable on steep terrain, where the ground return is ambiguous. Therefore, we do not consider steep terrain during training, following prior work[9].

Optimization. The training set contains more than 114 million samples, rendering standard random access impractical. We randomly split the data into 20 equally sized subsets and convert each to the FFCV beton format[67] for efficient random access. In each epoch, the model trains on a single subset using quasi-random sampling. After every 20 epochs (one full pass through all subsets), we randomly permute the subset order. We train for 400 epochs in total, corresponding to 20 full passes over the complete training dataset.

Training is distributed across 8 AMD Instinct MI250X GPUs with an effective batch size of 4096. We use the Adam optimizer[68] with a maximum learning rate of 10^{-3}. The learning rate increases linearly from 10^{-6} to 10^{-3} during a warm-up phase of 5 subset-epochs, then decays to 10^{-6} following a cosine scheduler over the remaining 15 full-dataset passes.

4.4 Calibration using conformal prediction

The prediction intervals from the quantile regression need not be valid, that is, we have no guarantees that the fraction of true values falling within the predicted interval is indeed 90%[69, 70]. As a step towards rigorous coverage guarantees, we apply SCP[36, 71]. Given a calibration set $\mathcal{D}_{\mathrm{cal}}$ of n samples and nominal miscoverage level α, SCP constructs prediction sets guaranteed to achieve at least $1-\alpha$ *expected* coverage on test data. This holds under the assumption that the calibration data and the test data are exchangeable[38].

For each RH level k, we follow a signed-error conformal regression (SECR)[72] approach, conformalizing the predicted lower and upper quantiles $\hat{q}_k^{(0.05)}(\boldsymbol{x})$ and $\hat{q}_k^{(0.95)}(\boldsymbol{x})$ separately using two non-conformity score functions

$$s_k^{\mathrm{lo}}(\boldsymbol{x}, y) \coloneqq \hat{q}_k^{(0.05)}(\boldsymbol{x}) - y, \quad s_k^{\mathrm{hi}}(\boldsymbol{x}, y) \coloneqq y - \hat{q}_k^{(0.95)}(\boldsymbol{x}), \tag{5}$$

evaluated on $\mathcal{D}_{\mathrm{cal}}$ at miscoverage levels $\alpha_{\mathrm{lo}} = \alpha_{\mathrm{hi}} = 0.05$. The resulting conformal corrections c_k^{lo} and c_k^{hi} are the empirical quantiles of each score distribution on $\mathcal{D}_{\mathrm{cal}}$, producing the prediction interval

$$\mathcal{C}_k(\boldsymbol{x}) = \left[\hat{q}_k^{(0.05)}(\boldsymbol{x}) - c_k^{\mathrm{lo}},\ \hat{q}_k^{(0.95)}(\boldsymbol{x}) + c_k^{\mathrm{hi}}\right], \tag{6}$$

satisfying

$$1 - \alpha_{\mathrm{lo}} - \alpha_{\mathrm{hi}} \le \mathbb{P}\left(\mathrm{RH}_k \in \mathcal{C}_k\left(\boldsymbol{X}\right)\right) \le 1 - \alpha_{\mathrm{lo}} - \alpha_{\mathrm{hi}} + \frac{1}{n+1} + \epsilon_{\mathrm{tie}}, \tag{7}$$

where RH_k and $\boldsymbol{X}$ are random variables. Here, ϵ_{tie} is the probability that the non-conformity score of a test data point is the same as the score of an element in the calibration set[73].

This two-sided guarantee, which bounds underprediction and overprediction independently, is the primary motivation for SECR over other popular conformal regression methods, such as conformalized quantile regression[74], where the total miscoverage can be arbitrarily distributed between the two tails.

Since quantile regression provides no monotonicity guarantee, predicted quantiles are sorted in increasing order prior to calibration, following[75]. We apply this calibration independently for each RH metric k and each WWF terrestrial biome $b \in \mathcal{B}$[39], an approach known as Mondrian conformal prediction[38]. Formally, corrections $c^{\mathrm{lo}}_{k,b}$ and $c^{\mathrm{hi}}_{k,b}$ are computed on the biome-stratified subset $\mathcal{D}^{b}_{\mathrm{cal}} \subset \mathcal{D}_{\mathrm{cal}}$ for each k separately. Since biomes are non-overlapping, this recovers both per-biome and global coverage guarantees simultaneously. Samples not falling within any biome are excluded from calibration. Since GEDI's orbital inclination restricts observations to within $\pm 51.6^{\circ}$ of the equator, the Tundra biome is represented by only 24 calibration samples, which is insufficient to yield reliable corrections; we therefore exclude it from calibration. Unlike during model training, calibration data is not filtered by slope, ensuring valid uncertainty estimates across all terrain conditions encountered in global deployment.

A single global correction can simultaneously overcover some biomes while leaving others systematically undercovered. Where calibration falls short of 90%, this reflects finite-sample limitations arising from the spatial structure of the data. Because the calibration and test sets were partitioned by large spatial tiles, samples from the same biome in each set may originate from geographically distant regions. Spatial autocorrelation within biomes implies that such samples are not fully exchangeable, reducing the effective calibration sample size below the nominal count and weakening the coverage guarantee.

In Extended Data Fig. A1 we show how conformal calibration affects the average interval width. The magnitude of the interval width adjustment reflects the degree of initial miscalibration in each stratum (Fig. **??**). Biomes characterized by severe undercoverage, most notably Montane grassland and Tropical coniferous forest, require the largest interval expansions, with average width increases of up to $8\,\mathrm{m}$ for upper canopy RH metrics. Conversely, biomes in which the uncalibrated model already overcovers (e.g., Tropical and Flooded grasslands) undergo modest interval contractions, improving the sharpness of the uncertainty estimates. The trend of increasing interval width with RH level reflects the growing marginal variance of the target distribution. Whereas RH0 is approximately anchored to ground level and exhibits little cross-sample variability, higher RH metrics span an increasingly wide range of values across heterogeneous global landscapes, requiring wider prediction intervals to maintain the target coverage.

An analogous mechanism accounts for the wider intervals in forest biomes compared to grasslands and deserts. Nevertheless, across this division, the degree of miscalibration is not uniform, and terrain slope is its primary driver. Model training was restricted to GEDI footprints on slopes not exceeding 20°. The calibration set, however, was not filtered by slope to provide valid uncertainty estimates across all terrain conditions encountered in global deployment. Consequently, steep-slope regions represent a form of covariate shift between training and calibration, and conformal prediction compensates for this by inflating predicted intervals in affected biomes, especially those with complex topography, such as Montane grassland. This behaviour illustrates a key strength of the conformal framework: it can extend valid uncertainty coverage to regions where the predictive model alone is poorly specified by absorbing these discrepancies into wider but statistically valid uncertainty bounds.

4.5 Evaluation

We evaluate our VSM against held-out GEDI footprints across the full RH profile. For visual clarity, we group RH metrics into bins of ten. For each RH group, we compare the distribution of our VSM with GEDI reference in a two-sided violin plot and the distribution of residuals using a boxplot.

We evaluate model performance using five complementary metrics. For continuous predictions such as individual RH metrics in the RH profile and derived diversity indices, we report RMSE, mean absolute error (MAE), and mean error (ME). RMSE captures the overall magnitude of prediction errors, with greater sensitivity to large deviations. MAE provides a more robust measure of average error magnitude. ME quantifies systematic bias, where negative values indicate underestimation, that is, predictions are systematically lower than the reference values. To assess the strength of agreement, we additionally report the coefficient of determination R^2: against GEDI and WSCI for structural complexity, and against airborne LiDAR references (ALS and LVIS) for canopy top height. For the downstream task on naturalness mapping, we report the F1 score, which balances precision and recall into a single classification performance measure.

Independent airborne LiDAR data. We evaluate the top height estimates of our VSM with independent airborne laser scanning data from multiple airborne campaigns within and beyond the GEDI coverage using the airborne reference data as reported in prior work[8]. Such ALS data are not systematically available at global scales due to the high costs and limited scalability. However, the high quality measurements of such airborne campaigns enable an independent validation of our approach. We use reference data from two sources including i) NASA's Land, Vegetation, and Ice Sensor (LVIS) airborne LiDAR campaigns[76], a large-footprint full-waveform LiDAR and ii) small-footprint airborne laser scanning (ALS) campaigns in Europe[53]. The latter has been processed to obtain GEDI-like canopy-top heights within a 25-meter footprint derived from high-resolution rastered canopy height models[8]. To minimize the temporal

discrepancy of potential land use changes between our VSM estimates and the ALS campaigns, we compute local annual VSMs for the years that match the airborne campaigns best back to 2017 when Sentinel-2 was fully operational. The results for 24 regions from different Sentinel-2 tiles are shown in Extended Data Fig. A2 and summarized in Extended Data Table A2. Our model achieved good overall agreement with both references, with R^2 values of 0.75 for LVIS and 0.64 for ALS. For most regions, our VSM achieved moderate to good agreement with the reference data, with per-tile R^2 ranging from 0.33 to 0.71 for LVIS and 0.31 to 0.77 for ALS. In four regions, our evaluation yielded negative R^2 values, which coincide with regions where visual inspection reveals land-use changes between the year of the airborne campaign and our map product (e.g. deforestation or tree harvesting). We observe a systematic relationship between average canopy height and model bias, that is, the model tends to slightly overestimate shorter vegetation while underestimating taller canopies, being a common limitation of canopy height maps derived from optical satellite imagery[8]. Overall, our model generalizes well across years as the CNN was trained on paired Sentinel-2 and GEDI data spanning four years from 2019–2022.

Uncertainty calibration. In addition to prediction accuracy, we evaluate the calibration of prediction intervals from conformal prediction. The empirical coverage of conformalized predictions for each biome b and RH metric k is given by

$$\widehat{\mathrm{Cov}}_{k,b} = \frac{1}{|\mathcal{D}^b_{\mathrm{test}}|} \sum_{(\boldsymbol{x},\mathrm{RH}) \in \mathcal{D}^b_{\mathrm{test}}} \left[\!\!\left[\mathrm{RH}_k \in \left[\hat{q}_k^{(0.05)}(\boldsymbol{x}) - c^{\mathrm{lo}}_{k,b},\, \hat{q}_k^{(0.95)}(\boldsymbol{x}) + c^{\mathrm{hi}}_{k,b} \right] \right]\!\!\right], \tag{8}$$

where $\hat{q}_k^{(0.95)}$ and $\hat{q}_k^{(0.05)}$ are predicted quantiles, $c^{\mathrm{lo}}_{k,b}$ and $c^{\mathrm{hi}}_{k,b}$ are the corresponding conformal corrections, and $[\![\cdot]\!]$ denotes the Iverson bracket. Initial empirical coverage is computed on predicted quantiles without the conformal corrections. The global empirical coverage for RH k is computed as

$$\widehat{\mathrm{Cov}}_k = \frac{1}{\sum_{b\in\mathcal{B}} |\mathcal{D}^b_{\mathrm{test}}|} \sum_{b\in\mathcal{B}} |\mathcal{D}^b_{\mathrm{test}}| \cdot \widehat{\mathrm{Cov}}_{k,b}. \tag{9}$$

Similarly, the average interval width for a given biome b and RH level k is given by

$$\overline{W}_{k,b} = \frac{1}{|\mathcal{D}^b_{\mathrm{test}}|} \sum_{(\boldsymbol{x},\mathrm{RH}) \in \mathcal{D}^b_{\mathrm{test}}} \left(\left(\hat{q}_k^{(0.95)}(\boldsymbol{x}) + c^{\mathrm{hi}}_{k,b} \right) - \left(\hat{q}_k^{(0.05)}(\boldsymbol{x}) - c^{\mathrm{lo}}_{k,b} \right) \right). \tag{10}$$

Comparison to state-of-the-art canopy top height maps. We show that the VSM improves the state of the art of top height estimates globally for the year 2020 by comparing against four recent products UMD[7], ETH[8], UM[9], and META[50], which use different canopy top height proxies. The modeling approaches of these products combined GEDI with different predictor data: While ETH used Sentinel-2, UM uses Sentinel-2 plus Sentinel-1, UMD relied on Landsat analyses ready data, and META had access to commercial 0.5 m resolution imagery from Maxar Technologies. Consequently, ETH and UM provide canopy top height estimates rastered at 10 m resolution. For a fair comparison, we resampled the UMD map from 30 m to 10 m using nearest-neighbor interpolation. We derive GEDI-like height estimates from the META map by max-pooling the 1 m resolution map according to GEDI's 25 m circular footprint. We show that our VSM is highly competitive and advances the state of the art in canopy top height estimation at 10 m resolution. The random errors naturally grow with higher RH metrics for our VSM product. On these overall metrics, our VSM yields a lower random error (RMSE, MAE) and bias (ME) compared to all products and yields a similar MAE as the UM map for RH100. We find that all existing products tend to have an underestimation bias, which is lowest for the ETH map and strongest for the META map (-3.54 m), despite our max-pooling processing.

Qualitatively, we find that our VSM substantially improves the quality in tropical and frequently cloudy regions (see Extended Data Fig. A5 column A-D). This is likely a result of our late aggregation strategy adapted from Lang et al.[8], which aggregates predictions based on individual Sentinel-2 images. While other work relies on mosaics of the input data, our approach can make use of any cloud-free pixel without propagating errors from input mosaics. Furthermore, giving the CNN access to the raw individual satellite imagery avoids any blurring effects in the input, which can arise when aggregating Sentinel-2 images that have sub-pixel misalignments[77].

4.6 Global map prediction

Sentinel-2 tile-level growing season. To ensure that the deployment data follow the same seasonal distribution as the training images, we aggregate pixel-level phenology to the Sentinel-2 tile level to determine the growing-season months associated with each tile. We derive phenological timing from VIIRS land surface phenology data, the same source used for `leaf_on_day` and `leaf_off_day` in GEDI attributes. For each tile, we compute the fraction of pixels whose growing season overlaps with a given month, relative to the number of pixels with valid VIIRS phenology data. The month is then classified as a growing month for the tile if this fraction exceeds 0.5. We restrict the calculation to pixels

with valid phenology observations to reduce the influence of non-vegetated areas and other locations where seasonal timing cannot be reliably estimated.

Input images. We produce wall-to-wall predictions for 2020 and 2024, covering all Sentinel-2 tiles over the Earth's landmass excluding Antarctica. We find 18,110 tiles with image coverage for 2020 and 18,144 for 2024. For each tile, we sample a compact set of cloud-free images acquired during the growing season that jointly provide full spatial coverage, this is achieved through a three-stage filtering pipeline. First, we query all Sentinel-2 images for the tile with cloud cover and no-data pixel percentage $\leq 90\%$ and captured within the growing months we precomputed. Second, to ensure full tile coverage, we retain all images from orbits with zero no-data pixels. Since spatial coverage is largely determined by orbit geometry, it remains nearly constant across acquisitions from the same orbit. For the remaining orbits, we take at most two with the least no-data pixel percentage and select the 10 most cloud-free images from each orbit. Finally, image candidates are ranked first by no-data percentage and then by cloud cover, and the top 20 images are selected. This yields a maximum of 20 images per tile.

Patch size and overlap. During inference, we first zero-pad each Sentinel-2 tile with 16 pixels on all sides. A sliding window of 544×544 pixels is then applied with a stride of 512 pixels, resulting in a 32-pixel overlap between adjacent patches. When reassembling the full tile, the outer 16-pixel border of each prediction patch is discarded, retaining only the central 512×512 pixels. This removes predictions affected by padding near patch boundaries and ensures that all retained predictions are made using real observations rather than padded values, and that neighboring patches share similar context along their borders, reducing border artifacts.

Post-inference median aggregation. For each Sentinel-2 tile, we adopt a post-inference median aggregation strategy. The model predicts the RH profile independently for each input image, and the final estimate is obtained as the per-pixel median across all predictions. Compared to aggregating the input images prior to inference, this approach better preserves fine-grained spatial details that may be attenuated by compositing inputs with varying atmospheric and illumination conditions. It also enables image-specific prediction quality masking, as different images are affected by different transient conditions. We apply snow, ice, and cloud masks before median aggregation and water and built-up masks after. The same masks are applied to each prediction as they may vary across acquisitions, while water and built-up areas remain largely unchanged within a single year. The image-specific snow, ice, and cloud masks are obtained as the union of cloud shadow, medium- and high-probability cloud, snow, and no-data classes from the Scene Classification Layer (SCL), together with snow and ice classes predicted by the land-cover head. The water bodies and built-up masks are obtained from a majority vote across all land-cover predictions. This majority vote reduces the influence of occasional misclassifications in individual predictions. The resulting water and built-up masks are applied to the median-aggregated RH profile prediction. Non-vegetated land surfaces such as bare ground and deserts are not masked and retain their predicted RH profiles. This preserves estimates in areas with sparse or low vegetation that may still carry meaningful structural information.

Postprocessing. A sliding window with overlap effectively removes the border artifacts within a tile. However, applying the same approach to neighboring tiles can lead to seamlines because adjacent tiles are often predicted from different image sets acquired at different times, and jointly processing neighboring tiles would substantially increase computational costs. Instead, we perform a post-inference blending step that computes a weighted average over overlapping areas between tiles. For each overlapping pixel, weights are computed from the distance to the corresponding tile boundary and normalized across all contributing tiles.

We round our predictions to decimeter precision and store them as int16 for better compression, therefore reducing storage space required. The accuracy loss relative to centimeter precision is less than 1 cm in MAE and ME. The final product is distributed at 10 m spatial resolution in UTM projection, consistent with the native Sentinel-2 tiling scheme, and stored as Cloud Optimized GeoTIFFs (COGs). Global inference for a single year was completed in approximately 5,000 GPU-hours on AMD Instinct MI250X GPUs, with an additional 228,000 CPU-hours for postprocessing and translation to COG format.

4.7 Deriving structural diversity indices from the VSM

Structural complexity or diversity indices are often derived to describe the vertical heterogeneity of vegetation and facilitate ecological interpretations. Here, we derived four diversity indices from the VSM profile: foliage height diversity (FHD)[40] as well as one- and two-dimensional effective number of layers (1D and 2D ENL)[42] and canopy ratio (CR)[43]. These are used in the following section as ablations to characterize forest naturalness and were computed from the predicted median RH metrics at pixel-level. For each pixel, the RH profile was converted into an approximate vertical distribution by aggregating RH values into discrete height bins. We retained finite and positive RH values, and discretized the vertical profile into 5 m height bins, which is consistent with the vertical bins used in the GEDI L2B vegetation structure product[4, 78]. Heights above 150 m were clipped, which removes values beyond the maximum

vegetation height expected globally and ensures a fixed vertical support for all calculations. The resulting histogram was normalized by the total count, and the result is viewed as a discrete probability distribution p over the vertical profile bins.

Foliage height diversity was then calculated as the Shannon entropy of this vertical distribution:

$$\text{FHD} = -\sum_{i=1}^{N} p_i \log p_i \tag{11}$$

Here, p_i refers to the probability of bin i and N refers to the number of bins. Bins with $p_i = 0$ were ignored. Following[42], 1D ENL was computed as the exponential of FHD

$$\text{1D ENL} = \exp\big(-\sum_{i=1}^{N} p_i \log p_i\big) \tag{12}$$

and 2D ENL was computed as the inverse Simpson concentration

$$\text{2D ENL} = 1/\sum_{i=1}^{N} p_i^2. \tag{13}$$

The effective number of layers was originally proposed for quantifying three-dimensional stand structure from terrestrial laser scanning using 1 m vertical layers. Here, we adapt the same Hill-number interpretation to VSM-derived RH profiles, while using 5 m bins to match the vertical discretization of GEDI L2B vegetation structure metrics[4].

Finally, the canopy ratio CR was computed as

$$\text{CR} = \frac{\text{RH98} - \text{RH25}}{\text{RH98}} \tag{14}$$

for $\text{RH98} > 0$. Before computing CR, negative RH25 values were clipped to zero because negative lower RH estimates have no physical interpretation as vegetation height above ground.

The FHD quantifies the vertical distribution of vegetation occupancy and increases with the evenness of vegetation occupancy across height layers. The ENL provides a complementary indicator by expressing vertical complexity as the equivalent number of equally occupied layers. Both 1D ENL and 2D ENL increase as vegetation becomes more evenly distributed across height layers, but 2D ENL places greater emphasis on dominant layers than 1D ENL. The CR reflects the relative separation between lower and upper canopy strata. It is sensitive to the degree of canopy closure and understory development. Together, these indices capture complementary aspects of vegetation structural complexity, including vertical heterogeneity, canopy layering, and the relative distribution of vegetation between lower and upper canopy strata. Such structural attributes have been linked to habitat quality, niche diversity, and biodiversity patterns across ecosystems[43, 79].

4.8 Natural forest classification as a downstream task

VSM-based classification. Vertical vegetation structure varies systematically across forest types shaped by different management histories and disturbances.[80] showed that unmanaged naturally regenerating forests develop canopy structures approaching those of intact forests, whereas managed regenerating and planted forests diverge considerably. Primary forests typically develop multi-layered canopies with high structural complexity, whereas planted forests tend to exhibit uniform, single-layer canopy profiles[46]. While optical imagery implicitly encodes information related to canopy structure, this signal is distributed across spectral bands and entangled with confounding factors such as phenology and illumination conditions. The VSM distills this information into an explicit vertical profile, providing a representation that a classifier can leverage more directly for tasks where structural differences are discriminative.

To evaluate whether the VSM captures structural information beyond canopy top height, we use the expert-annotated forest management labels from[35], which comprise seven classes: natural forest, natural forest (secondary), agroforestry, planted forest, short rotation plantation, oil palm, and no forest. We randomly split the labeled samples into 80% for training and 20% for testing. Two questions guide the experiments: (i) does the spatially dense VSM add value over point-wise vertical profiles? (ii) does the full vertical profile carry discriminative information beyond canopy top height (RH98)?

We address both questions with two classifiers of increasing expressiveness: a logistic regression, which isolates the contribution of individual input features in a linear setting, and a CNN using the same architecture as for VSM prediction

with the regression head replaced by a classification head trained with cross-entropy loss. For the logistic regression, we extract per-pixel features at forest management label locations. For the CNN, we use spatially dense VSM predictions as input, enabling the model to exploit spatial context from neighboring pixels. To systematically assess the contribution of vertical structure, we compare the following input configurations under both classifiers: i) *RH98 only*: canopy top height as a baseline, ii) *RH98 + individual diversity indices (FHD, 2D ENL, CR)*: testing whether common summary measures of vertical complexity improve upon top height, iii) *RH98 + key RH metrics (RH25, RH50, RH75, RH90, RH95)*: testing whether few key RH metrics complement top height, iv) *Full profile (RH0–RH100)*: the complete 101-channel vertical structure representation, v) *RH98 + Sentinel-2* — testing the complementarity of canopy top height and spectral data, vi) *Full profile + Sentinel-2*: testing the complementarity of the VSM and spectral data.

The CNN uses the same optimizer and cosine annealing schedule as for VSM prediction, with a maximum learning rate of 1×10^{-4}, a batch size of 1024, and is trained for 200 epochs on 15×15 pixel input patches. We report macro-averaged F1 across all classes as well as per-class F1 scores. We do not apply class weighting or oversampling to address the class imbalance present in the reference labels, as macro-averaged F1 inherently weights all classes equally regardless of prevalence.

To isolate the effect of spatial context, we additionally compare the logistic regression classifier operating on spatially dense VSM grids against the same model operating on point-wise profiles sampled at GEDI footprint locations (Fig. 13a).

Supplementary information

Data availability The complete VSM data (full relative height profile) for 2020 and 2024 is hosted at Source Cooperative (`https://source.coop/geoai-ucph/gvsm`; DOI forthcoming).

We also provide 15 key RH metrics at global scale, available at CloudFerro (`https://s3.waw4-1.cloudferro.com/vsm-data-public/`). For both repositories, data upload is ongoing and will be complete upon publication.

We have created a data viewer that allows to inspect the data globally: `https://huizhml.github.io/map-explorer/`

Code availability Details will be provided in a later version of this manuscript.

Acknowledgments HZ, KH, MB, RF, AK, and CI acknowledge support from the Danish National Research Foundation (DNRF), Center for Remote Sensing and Deep Learning of Global Tree Resources (TreeSense), grant number DNRF192. NL, SO, RF, and CI acknowledge support from the Novo Nordisk Foundation, Global Wetland Center (GWC), grant number NNF23OC0081089. MM acknowledges support from the DNRF, Pioneer Centre for AI, grant number P1. KH acknowledges support from the Innovation Fond Denmark, Innovative forests for curbing climate change while integrating biodiversity, nutrient retention, and recreation (INNO4EST). We acknowledge University of Copenhagen, Denmark for awarding this project access to the LUMI supercomputer, owned by the EuroHPC Joint Undertaking, hosted by CSC (Finland) and the LUMI consortium through University of Copenhagen, Denmark. We gratefully acknowledge both Source Cooperative and CloudFerro for supporting this project with generous cloud storage to host the VSM data product.

References

[1] Stuart L Pimm, Clinton N Jenkins, and Binbin V Li. How to protect half of Earth to ensure it protects sufficient biodiversity. *Science Advances*, 4(8):eaat2616, 2018.

[2] Bernardo BN Strassburg, Alvaro Iribarrem, Hawthorne L Beyer, Carlos Leandro Cordeiro, Renato Crouzeilles, Catarina C Jakovac, André Braga Junqueira, Eduardo Lacerda, Agnieszka E Latawiec, Andrew Balmford, et al. Global priority areas for ecosystem restoration. *Nature*, 586(7831):724–729, 2020.

[3] Martin Jung, Andy Arnell, Xavier De Lamo, Shaenandhoa García-Rangel, Matthew Lewis, Jennifer Mark, Cory Merow, Lera Miles, Ian Ondo, Samuel Pironon, et al. Areas of global importance for conserving terrestrial biodiversity, carbon and water. *Nature Ecology & Evolution*, 5(11):1499–1509, 2021.

[4] Ralph Dubayah, James Bryan Blair, Scott Goetz, Lola Fatoyinbo, Matthew Hansen, Sean Healey, Michelle Hofton, George Hurtt, James Kellner, Scott Luthcke, et al. The global ecosystem dynamics investigation: High-resolution laser ranging of the earth's forests and topography. *Science of remote sensing*, 1:100002, 2020.

[5] Tiago de Conto, John Armston, and Ralph Dubayah. Characterizing the structural complexity of the Earth's forests with spaceborne lidar. *Nature Communications*, 15(1):8116, 2024.

[6] Mirco Migliavacca, Talie Musavi, Miguel D Mahecha, Jacob A Nelson, Jürgen Knauer, Dennis D Baldocchi, Oscar Perez-Priego, Rune Christiansen, Jonas Peters, Karen Anderson, et al. The three major axes of terrestrial ecosystem function. *Nature*, 598(7881):468–472, 2021.

[7] Peter Potapov, Xinyuan Li, Andres Hernandez-Serna, Alexandra Tyukavina, Matthew C. Hansen, Anil Kommareddy, Amy Pickens, Svetlana Turubanova, Hao Tang, Carlos Edibaldo Silva, John Armston, Ralph Dubayah, J. Bryan Blair, and Michelle Hofton. Mapping global forest canopy height through integration of GEDI and Landsat data. *Remote Sensing of Environment*, 253:112165, February 2021. ISSN 0034-4257. doi:10.1016/j.rse.2020.112165. URL https://www.sciencedirect.com/science/article/pii/S0034425720305381.

[8] Nico Lang, Walter Jetz, Konrad Schindler, and Jan Dirk Wegner. A high-resolution canopy height model of the Earth. *Nature Ecology & Evolution*, 7(11):1778–1789, November 2023. ISSN 2397-334X. doi:10.1038/s41559-023-02206-6. URL https://www.nature.com/articles/s41559-023-02206-6.

[9] Jan Pauls, Max Zimmer, Una M. Kelly, Martin Schwartz, Sassan Saatchi, Philippe Ciais, Sebastian Pokutta, Martin Brandt, and Fabian Gieseke. Estimating canopy height at scale. In Ruslan Salakhutdinov, Zico Kolter, Katherine Heller, Adrian Weller, Nuria Oliver, Jonathan Scarlett, and Felix Berkenkamp, editors, *Proceedings of the 41st International Conference on Machine Learning*, volume 235 of *Proceedings of Machine Learning Research*, pages 39972–39988. PMLR, 21–27 Jul 2024. URL https://proceedings.mlr.press/v235/pauls24a.html.

[10] Elizabeth Maruma Mrema, Thomas W Crowther, Wanjira Mathai, Thomas Brooks, Sally Archibald, Pedro Brancalion, Edward B Barbier, David Obura, Victoria Reyes-García, William J Bond, et al. Ten years to restore a planet. *One Earth*, 3(6):647–652, 2020.

[11] Global Biodiversity Framework. Kunming-Montreal global biodiversity framework. Convention on Biological Diversity, 2022.

[12] Christopher L Gilbert. The EU deforestation regulation. *EuroChoices*, 23(3):64–70, 2024.

[13] Peter Manning, Fons Van Der Plas, Santiago Soliveres, Eric Allan, Fernando T Maestre, Georgina Mace, Mark J Whittingham, and Markus Fischer. Redefining ecosystem multifunctionality. *Nature Ecology & Evolution*, 2(3): 427–436, 2018.

[14] James EM Watson, Tom Evans, Oscar Venter, Brooke Williams, Ayesha Tulloch, Claire Stewart, Ian Thompson, Justina C Ray, Kris Murray, Alvaro Salazar, et al. The exceptional value of intact forest ecosystems. *Nature Ecology & Evolution*, 2(4):599–610, 2018.

[15] Tara G Martin and James EM Watson. Intact ecosystems provide best defence against climate change. *Nature Climate Change*, 6(2):122–124, 2016.

[16] Karina Winkler, Richard Fuchs, Mark Rounsevell, and Martin Herold. Global land use changes are four times greater than previously estimated. *Nature communications*, 12(1):2501, 2021.

[17] Nguyen Tien Hoang and Keiichiro Kanemoto. Mapping the deforestation footprint of nations reveals growing threat to tropical forests. *Nature Ecology & Evolution*, 5(6):845–853, 2021.

[18] Nikolai Kalischek, Nico Lang, Cécile Renier, Rodrigo Caye Daudt, Thomas Addoah, William Thompson, Wilma J Blaser-Hart, Rachael Garrett, Konrad Schindler, and Jan D Wegner. Cocoa plantations are associated with deforestation in côte d'ivoire and ghana. *Nature Food*, 4(5):384–393, 2023.

[19] Wang Li, Wen-Yong Guo, Maya Pasgaard, Zheng Niu, Li Wang, Fang Chen, Yuchu Qin, and Jens-Christian Svenning. Human fingerprint on structural density of forests globally. *Nature Sustainability*, 6(4):368–379, April 2023. ISSN 2398-9629. doi:10.1038/s41893-022-01020-5. URL https://www.nature.com/articles/s41893-022-01020-5.

[20] Kendall R Jones, Oscar Venter, Richard A Fuller, James R Allan, Sean L Maxwell, Pablo Jose Negret, and James EM Watson. One-third of global protected land is under intense human pressure. *Science*, 360(6390): 788–791, 2018.

[21] IPBES. *Global Assessment Report on Biodiversity and Ecosystem Services of the Intergovernmental Science-Policy Platform on Biodiversity and Ecosystem Services*. IPBES Secretariat, Bonn, Germany, 2019. doi:10.5281/zenodo.3831673. URL https://doi.org/10.5281/zenodo.3831673.

[22] Moreno Di Marco, Stuart HM Butchart, Piero Visconti, Graeme M Buchanan, Gentile F Ficetola, and Carlo Rondinini. Synergies and trade-offs in achieving global biodiversity targets. *Conservation Biology*, 30(1):189–195, 2016.

[23] Sarah R Weiskopf, Forest Isbell, Maria Isabel Arce-Plata, Moreno Di Marco, Mike Harfoot, Justin Johnson, Susannah B Lerman, Brian W Miller, Toni Lyn Morelli, Akira S Mori, et al. Biodiversity loss reduces global terrestrial carbon storage. *Nature Communications*, 15(1):4354, 2024.

[24] Alessandro Chiarucci and Gianluca Piovesan. Need for a global map of forest naturalness for a sustainable future. *Conservation Biology*, 34(2):368–372, 2020.

[25] Lidong Mo, Constantin M Zohner, Peter B Reich, Jingjing Liang, Sergio De Miguel, Gert-Jan Nabuurs, Susanne S Renner, Johan Van Den Hoogen, Arnan Araza, Martin Herold, et al. Integrated global assessment of the natural forest carbon potential. *Nature*, 624(7990):92–101, 2023.

[26] Laura Duncanson, James R. Kellner, John Armston, Ralph Dubayah, David M. Minor, Steven Hancock, Sean P. Healey, Paul L. Patterson, Svetlana Saarela, Suzanne Marselis, Carlos E. Silva, Jamis Bruening, Scott J. Goetz, Hao Tang, Michelle Hofton, Bryan Blair, Scott Luthcke, Lola Fatoyinbo, Katharine Abernethy, Alfonso Alonso, Hans-Erik Andersen, Paul Aplin, Timothy R. Baker, Nicolas Barbier, Jean Francois Bastin, Peter Biber, Pascal Boeckx, Jan Bogaert, Luigi Boschetti, Peter Brehm Boucher, Doreen S. Boyd, David F. R. P. Burslem, Sofia Calvo-Rodriguez, Jérôme Chave, Robin L. Chazdon, David B. Clark, Deborah A. Clark, Warren B. Cohen, David A. Coomes, Piermaria Corona, K. C. Cushman, Mark E. J. Cutler, James W. Dalling, Michele Dalponte, Jonathan Dash, Sergio de Miguel, Songqiu Deng, Peter Woods Ellis, Barend Erasmus, Patrick A. Fekety, Alfredo Fernandez-Landa, Antonio Ferraz, Rico Fischer, Adrian G. Fisher, Antonio García-Abril, Terje Gobakken, Jorg M. Hacker, Marco Heurich, Ross A. Hill, Chris Hopkinson, Huabing Huang, Stephen P. Hubbell, Andrew T. Hudak, Andreas Huth, Benedikt Imbach, Kathryn J. Jeffery, Masato Katoh, Elizabeth Kearsley, David Kenfack, Natascha Kljun, Nikolai Knapp, Kamil Král, Martin Krůček, Nicolas Labrière, Simon L. Lewis, Marcos Longo, Richard M. Lucas, Russell Main, Jose A. Manzanera, Rodolfo Vásquez Martínez, Renaud Mathieu, Herve Memiaghe, Victoria Meyer, Abel Monteagudo Mendoza, Alessandra Monerris, Paul Montesano, Felix Morsdorf, Erik Næsset, Laven Naidoo, Reuben Nilus, Michael O'Brien, David A. Orwig, Konstantinos Papathanassiou, Geoffrey Parker, Christopher Philipson, Oliver L. Phillips, Jan Pisek, John R. Poulsen, Hans Pretzsch, Christoph Rüdiger, Sassan Saatchi, Arturo Sanchez-Azofeifa, Nuria Sanchez-Lopez, Robert Scholes, Carlos A. Silva, Marc Simard, Andrew Skidmore, Krzysztof Stereńczak, Mihai Tanase, Chiara Torresan, Ruben Valbuena, Hans Verbeeck, Tomas Vrska, Konrad Wessels, Joanne C. White, Lee J. T. White, Eliakimu Zahabu, and Carlo Zgraggen. Aboveground biomass density models for NASA's Global Ecosystem Dynamics Investigation (GEDI) lidar mission. *Remote Sensing of Environment*, 270:112845, March 2022. ISSN 0034-4257. doi:10.1016/j.rse.2021.112845. URL `https://www.sciencedirect.com/science/article/pii/S0034425721005654`.

[27] Suzanne M Marselis, Petr Keil, Jonathan M Chase, and Ralph Dubayah. The use of gedi canopy structure for explaining variation in tree species richness in natural forests. *Environmental Research Letters*, 17(4):045003, 2022.

[28] Suzanne Mariëlle Marselis, Hao Tang, John Armston, Katharine Abernethy, Alfonso Alonso, Nicolas Barbier, Pulchérie Bissiengou, Kathryn Jeffery, David Kenfack, Nicolas Labrière, et al. Exploring the relation between remotely sensed vertical canopy structure and tree species diversity in gabon. *Environmental Research Letters*, 14 (9):094013, 2019.

[29] Tristan RM Bakx, Zsófia Koma, Arie C Seijmonsbergen, and W Daniel Kissling. Use and categorization of light detection and ranging vegetation metrics in avian diversity and species distribution research. *Diversity and Distributions*, 25(7):1045–1059, 2019.

[30] Tiago de Conto, John Armston, and Ralph Dubayah. Scalable deep fusion of spaceborne lidar and synthetic aperture radar for global forest structural complexity mapping. *Machine Learning: Earth*, 2(1):015002, 2026.

[31] Martin Brandt, Jerome Chave, Sizhuo Li, Rasmus Fensholt, Philippe Ciais, Jean-Pierre Wigneron, Fabian Gieseke, Sass an Saatchi, Compton J. Tucker, and Christian Igel. High-resolution sensors and deep learning models for tree resource monitoring. *Nature Reviews Electrical Engineering*, 2:13–26, 2025.

[32] M. Girardello, G. Oton, M. Piccardo, M. Pickering, A. Elia, G. Ceccherini, M. Garcia, M. Migliavacca, and A. Cescatti. A dataset on the structural diversity of european forests. *Earth System Science Data*, 18(4):2667–2687, 2026. doi:10.5194/essd-18-2667-2026. URL `https://essd.copernicus.org/articles/18/2667/2026/`.

[33] Ibrahim Fayad, Nicolas Baghdadi, Clayton Alcarde Alvares, Jose Luiz Stape, Jean Stéphane Bailly, Henrique Ferraço Scolforo, Italo Ramos Cegatta, Mehrez Zribi, and Guerric Le Maire. Terrain slope effect on forest height and wood volume estimation from GEDI data. *Remote Sensing*, 13(11):2136, May 2021. ISSN 2072-4292. doi:10.3390/rs13112136. URL `https://www.mdpi.com/2072-4292/13/11/2136`.

[34] Wenjian Ni, Zhiyu Zhang, and Guoqing Sun. Assessment of slope-adaptive metrics of GEDI waveforms for estimations of forest aboveground biomass over mountainous areas. *Journal of Remote Sensing*, 2021, August 2021. doi:10.34133/2021/9805364. URL `https://spj.science.org/doi/10.34133/2021/9805364`.

[35] Myroslava Lesiv, Dmitry Schepaschenko, Marcel Buchhorn, Linda See, Martina Dürauer, Ivelina Georgieva, Martin Jung, Florian Hofhansl, Katharina Schulze, Andrii Bilous, Volodymyr Blyshchyk, Liudmila Mukhortova, Carlos Luis Muñoz Brenes, Leonid Krivobokov, Stephan Ntie, Khongor Tsogt, Stephan Alexander Pietsch,

Elena Tikhonova, Moonil Kim, Fulvio Di Fulvio, Yuan-Fong Su, Roma Zadorozhniuk, Flavius Sorin Sirbu, Kripal Panging, Svitlana Bilous, Sergii B. Kovalevskii, Florian Kraxner, Ahmed Harb Rabia, Roman Vasylyshyn, Rekib Ahmed, Petro Diachuk, Serhii S. Kovalevskyi, Khangsembou Bungnamei, Kusumbor Bordoloi, Andrii Churilov, Olesia Vasylyshyn, Dhrubajyoti Sahariah, Anatolii P. Tertyshnyi, Anup Saikia, Ziga Malek, Kuleswar Singha, Roman Feshchenko, Reinhard Prestele, Ibrar ul Hassan Akhtar, Kiran Sharma, Galyna Domashovets, Seth A. Spawn-Lee, Oleksii Blyshchyk, Oleksandr Slyva, Mariia Ilkiv, Oleksandr Melnyk, Vitalii Sliusarchuk, Anatolii Karpuk, Andrii Terentiev, Valentin Bilous, Kateryna Blyshchyk, Maxim Bilous, Nataliia Bogovyk, Ivan Blyshchyk, Sergey Bartalev, Mikhail Yatskov, Bruno Smets, Piero Visconti, Ian Mccallum, Michael Obersteiner, and Steffen Fritz. Global forest management data for 2015 at a 100 m resolution. *Scientific Data*, 9(1):199, May 2022. ISSN 2052-4463. doi:10.1038/s41597-022-01332-3. URL `https://www.nature.com/articles/s41597-022-01332-3`.

[36] Jing Lei, Max G'Sell, Alessandro Rinaldo, Ryan J. Tibshirani, and Larry Wasserman. Distribution-free predictive inference for regression. *Journal of the American Statistical Association*, 113(523):1094–1111, 2018. doi:10.1080/01621459.2017.1307116. URL `https://doi.org/10.1080/01621459.2017.1307116`.

[37] Anastasios N. Angelopoulos and Stephen Bates. Conformal prediction: A gentle introduction. *Foundations and Trends in Machine Learning*, 16(4):494–591, 2023. ISSN 1935-8237. doi:10.1561/2200000101.

[38] Vladimir Vovk, Alexander Gammerman, and Glenn Shafer. *Algorithmic Learning in a Random World*. Springer Cham, second edition, December 2022. ISBN 978-3-031-06648-1. doi:10.1007/978-3-031-06649-8.

[39] Eric Dinerstein, David Olson, Anup Joshi, Carly Vynne, Neil D. Burgess, Eric Wikramanayake, Nathan Hahn, Suzanne Palminteri, Prashant Hedao, Reed Noss, Matt Hansen, Harvey Locke, Erle C Ellis, Benjamin Jones, Charles Victor Barber, Randy Hayes, Cyril Kormos, Vance Martin, Eileen Crist, Wes Sechrest, Lori Price, Jonathan E. M. Baillie, Don Weeden, Kierán Suckling, Crystal Davis, Nigel Sizer, Rebecca Moore, David Thau, Tanya Birch, Peter Potapov, Svetlana Turubanova, Alexandra Tyukavina, Nadia de Souza, Lilian Pintea, José C. Brito, Othman A. Llewellyn, Anthony G. Miller, Annette Patzelt, Shahina A. Ghazanfar, Jonathan Timberlake, Heinz Klöser, Yara Shennan-Farpón, Roeland Kindt, Jens-Peter Barnekow Lillesø, Paulo van Breugel, Lars Graudal, Maianna Voge, Khalaf F. Al-Shammari, and Muhammad Saleem. An ecoregion-based approach to protecting half the terrestrial realm. *BioScience*, 67(6):534–545, 06 2017. ISSN 0006-3568. doi:10.1093/biosci/bix014. URL `https://doi.org/10.1093/biosci/bix014`.

[40] Robert H MacArthur and John W MacArthur. On bird species diversity. *Ecology*, 42(3):594–598, 1961.

[41] Rick Clawges, Kerri Vierling, Lee Vierling, and Eric Rowell. The use of airborne lidar to assess avian species diversity, density, and occurrence in a pine/aspen forest. *Remote sensing of environment*, 112(5):2064–2073, 2008.

[42] Martin Ehbrecht, Peter Schall, Julia Juchheim, Christian Ammer, and Dominik Seidel. Effective number of layers: A new measure for quantifying three-dimensional stand structure based on sampling with terrestrial lidar. *Forest Ecology and Management*, 380:212–223, 2016.

[43] Fabian D Schneider, António Ferraz, Steven Hancock, Laura I Duncanson, Ralph O Dubayah, Ryan P Pavlick, and David S Schimel. Towards mapping the diversity of canopy structure from space with GEDI. *Environmental Research Letters*, 15(11):115006, 2020.

[44] Erone Ghizoni Santos, Matheus Henrique Nunes, Toby Jackson, and Eduardo Eiji Maeda. Quantifying tropical forest disturbances using canopy structural traits derived from terrestrial laser scanning. *Forest Ecology and Management*, 524:120546, 2022.

[45] Maxim Neumann, Anton Raichuk, Yuchang Jiang, Mélanie Rey, Radost Stanimirova, Michelle J Sims, Sarah Carter, Elizabeth Goldman, Keith Anderson, Petra Poklukar, et al. Natural forests of the world–a 2020 baseline for deforestation and degradation monitoring. *Scientific Data*, 12(1):1715, 2025.

[46] Laura J. Hickey, Jeff Atkins, Robert T. Fahey, Mark R. Kreider, Shea B. Wales, and Christopher M. Gough. Contrasting Development of Canopy Structure and Primary Production in Planted and Naturally Regenerated Red Pine Forests. *Forests*, 10(7), July 2019. ISSN 1999-4907. doi:10.3390/f10070566. URL `https://www.mdpi.com/1999-4907/10/7/566`.

[47] Erone Ghizoni Santos, Martin Svátek, Matheus Henrique Nunes, Juha Aalto, Rebecca A. Senior, Radim Matula, Roman Plichta, and Eduardo Eiji Maeda. Structural changes caused by selective logging undermine the thermal buffering capacity of tropical forests. *Agricultural and Forest Meteorology*, 348:109912, April 2024. ISSN 0168-1923. doi:10.1016/j.agrformet.2024.109912. URL `https://www.sciencedirect.com/science/article/pii/S0168192324000273`.

[48] Christelle Vancutsem, Frédéric Achard, J-F Pekel, Ghislain Vieilledent, Silvia Carboni, Dario Simonetti, Javier Gallego, Luiz EOC Aragao, and Robert Nasi. Long-term (1990–2019) monitoring of forest cover changes in the humid tropics. *Science advances*, 7(10):eabe1603, 2021.

[49] Andrew K Skidmore, Nicholas C Coops, Elnaz Neinavaz, Abebe Ali, Michael E Schaepman, Marc Paganini, W Daniel Kissling, Petteri Vihervaara, Roshanak Darvishzadeh, Hannes Feilhauer, et al. Priority list of biodiversity metrics to observe from space. *Nature Ecology & Evolution*, 5(7):896–906, 2021.

[50] Jamie Tolan, Hung-I Yang, Benjamin Nosarzewski, Guillaume Couairon, Huy V. Vo, John Brandt, Justine Spore, Sayantan Majumdar, Daniel Haziza, Janaki Vamaraju, Theo Moutakanni, Piotr Bojanowski, Tracy Johns, Brian White, Tobias Tiecke, and Camille Couprie. Very high resolution canopy height maps from RGB imagery using self-supervised vision transformer and convolutional decoder trained on aerial lidar. *Remote Sensing of Environment*, 300:113888, January 2024. ISSN 0034-4257. doi:10.1016/j.rse.2023.113888. URL https://www.sciencedirect.com/science/article/pii/S003442572300439X.

[51] Rede Simex. Sistema de monitoramento da exploração madeireira (Simex): Mapeamento da exploração madeireira na amazônia – agosto 2020 a julho 2021. Technical report, Imazon, Idesam, Imaflora e ICV, Belém, Brazil, 2022. URL https://imazon.org.br/publicacoes/sistema-de-monitoramento-da-exploracao-madeireira-simex-mapeamento-da-exploracao-madeireira-na-amazonia-agosto-2020-a-julho-2021/.

[52] Shaun Quegan, Thuy Le Toan, Jerome Chave, Jorgen Dall, Jean-François Exbrayat, Dinh Ho Tong Minh, Mark Lomas, Mauro Mariotti D'alessandro, Philippe Paillou, Kostas Papathanassiou, et al. The european space agency biomass mission: Measuring forest above-ground biomass from space. *Remote Sensing of Environment*, 227: 44–60, 2019.

[53] Siyu Liu, Martin Brandt, Thomas Nord-Larsen, Jerome Chave, Florian Reiner, Nico Lang, Xiaoye Tong, Philippe Ciais, Christian Igel, Adrian Pascual, et al. The overlooked contribution of trees outside forests to tree cover and woody biomass across europe. *Science Advances*, 9(37):eadh4097, 2023.

[54] Fabien H Wagner, Sophia Roberts, Alison L Ritz, Griffin Carter, Ricardo Dalagnol, Samuel Favrichon, Mayumi CM Hirye, Martin Brandt, Philippe Ciais, and Sassan Saatchi. Sub-meter tree height mapping of california using aerial images and lidar-informed u-net model. *Remote Sensing of Environment*, 305:114099, 2024.

[55] Maxim Neumann, Anton Raichuk, Peter Potapov, Myroslava Lesiv, Matthew Overlan, Mélanie Rey, Ravindran Rajakumar, Michelangelo Conserva, Radost Stanimirova, Michelle Sims, et al. Global forest typology at 10-meter resolution for forest and land-use monitoring. *EarthArXiv preprint*, 2026.

[56] Laura J Pollock, Justin Kitzes, Sara Beery, Kaitlyn M Gaynor, Marta A Jarzyna, Oisin Mac Aodha, Bernd Meyer, David Rolnick, Graham W Taylor, Devis Tuia, et al. Harnessing artificial intelligence to fill global shortfalls in biodiversity knowledge. *Nature Reviews Biodiversity*, 1(3):166–182, 2025.

[57] Laura Duncanson, Neha Hunka, Tommaso Jucker, John Armston, Nancy Harris, Lola Fatoyinbo, Christopher A Williams, Jeff W Atkins, Brett Raczka, Shawn Serbin, et al. Spatial resolution for forest carbon maps. *Science*, 387(6732):370–371, 2025.

[58] Alessandro Baccini, Wayne Walker, Luis Carvalho, Mary Farina, Damien Sulla-Menashe, and Richard A Houghton. Tropical forests are a net carbon source based on aboveground measurements of gain and loss. *Science*, 358(6360): 230–234, 2017.

[59] Nico Lang, Nikolai Kalischek, John Armston, Konrad Schindler, Ralph Dubayah, and Jan Dirk Wegner. Global canopy height regression and uncertainty estimation from GEDI LIDAR waveforms with deep ensembles. *Remote Sensing of Environment*, 268:112760, January 2022. ISSN 0034-4257. doi:10.1016/j.rse.2021.112760. URL https://www.sciencedirect.com/science/article/pii/S0034425721004806.

[60] Kamel Lahssini, Nicolas Baghdadi, Guerric Le Maire, Stéphane Dupuy, and Ibrahim Fayad. Use of GEDI signal and environmental parameters to improve canopy height estimation over tropical forest ecosystems in Mayotte Island. *Canadian Journal of Remote Sensing*, 50(1):2351004, December 2024. ISSN 0703-8992. doi:10.1080/07038992.2024.2351004. URL https://doi.org/10.1080/07038992.2024.2351004.

[61] David P. Roy, Herve B. Kashongwe, and John Armston. The impact of geolocation uncertainty on GEDI tropical forest canopy height estimation and change monitoring. *Science of Remote Sensing*, 4:100024, December 2021. ISSN 2666-0172. doi:10.1016/j.srs.2021.100024. URL https://www.sciencedirect.com/science/article/pii/S2666017221000110.

[62] Gerhard Krieger, Alberto Moreira, Hauke Fiedler, Irena Hajnsek, Marian Werner, Marwan Younis, and Manfred Zink. Tandem-x: A satellite formation for high-resolution sar interferometry. *IEEE Transactions on Geoscience and Remote Sensing*, 45(11):3317–3341, 2007.

[63] François Chollet. Xception: Deep learning with depthwise separable convolutions. In Andrew Hoogs, Rama Chellappa, Zhengyou Zhang, James M. Rehg, Yizhou Yu, Yang Liu, and Charles J. Taylor, editors, *Computer Vision and Pattern Recognition (CVPR)*, pages 1251–1258, 2017.

[64] Nico Lang, Konrad Schindler, and Jan Dirk Wegner. Country-wide high-resolution vegetation height mapping with Sentinel-2. *Remote Sensing of Environment*, 233:111347, November 2019. ISSN 0034-4257. doi:10.1016/j.rse.2019.111347. URL https://www.sciencedirect.com/science/article/pii/S0034425719303669.

[65] Roger Koenker and Gilbert Bassett. Regression quantiles. *Econometrica*, 46(1):33–50, 1978.

[66] Ingo Steinwart and Andreas Christmann. Estimating conditional quantiles with the help of the pinball loss. *Bernoulli*, 17(1):211–225, 2011. doi:10.3150/10-BEJ267. URL https://doi.org/10.3150/10-BEJ267.

[67] Guillaume Leclerc, Andrew Ilyas, Logan Engstrom, Sung Min Park, Hadi Salman, and Aleksander Madry. FFCV: Accelerating training by removing data bottlenecks. In Andreas Geiger, Ross Girshick, Judy Hoffman, Vladlen Koltun, Svetlana Lazebnik, Michael S. Brown, Fei-Fei Li, Greg Mori, and Yoichi Sato, editors, *Computer Vision and Pattern Recognition (CVPR)*. arXiv, June 2023. URL http://arxiv.org/abs/2306.12517.

[68] Diederik P Kingma and Jimmy Ba. Adam: A method for stochastic optimization. In Yoshua Bengio and Yann LeCun, editors, *International Conference on Learning Representations (ICLR)*, 2015.

[69] Victor Dheur and Souhaib Ben Taieb. A large-scale study of probabilistic calibration in neural network regression. In Andreas Krause, Emma Brunskill, Kyunghyun Cho, Barbara Engelhardt, Sivan Sabato, and Jonathan Scarlett, editors, *Proceedings of the 40th International Conference on Machine Learning*, volume 202 of *Proceedings of Machine Learning Research*, pages 7813–7836. PMLR, 23–29 Jul 2023. URL https://proceedings.mlr.press/v202/dheur23a.html.

[70] Yu Bai, Song Mei, Huan Wang, and Caiming Xiong. Understanding the under-coverage bias in uncertainty estimation. In M. Ranzato, A. Beygelzimer, Y. Dauphin, P.S. Liang, and J. Wortman Vaughan, editors, *Advances in Neural Information Processing Systems*, volume 34, pages 18307–18319. Curran Associates, Inc., 2021. URL https://proceedings.neurips.cc/paper_files/paper/2021/file/9854d7afce413aa13cd0a1d39d0bcec5-Paper.pdf.

[71] Harris Papadopoulos, Kostas Proedrou, Volodya Vovk, and Alex Gammerman. Inductive confidence machines for regression. In Tapio Elomaa, Heikki Mannila, and Hannu Toivonen, editors, *Machine Learning: ECML 2002*, pages 345–356, Berlin, Heidelberg, 2002. Springer Berlin Heidelberg. ISBN 978-3-540-36755-0.

[72] Henrik Linusson, Ulf Johansson, and Tuve Löfström. Signed-error conformal regression. In Vincent S. Tseng, Tu Bao Ho, Zhi-Hua Zhou, Arbee L. P. Chen, and Hung-Yu Kao, editors, *Advances in Knowledge Discovery and Data Mining*, pages 224–236, Cham, 2014. Springer International Publishing. ISBN 978-3-319-06608-0.

[73] Anastasios N. Angelopoulos, Rina Foygel Barber, and Stephen Bates. *Theoretical Foundations of Conformal Prediction*. Cambridge University Press, Cambridge, UK, 2026. URL https://arxiv.org/abs/2411.11824. In press.

[74] Yaniv Romano, Evan Patterson, and Emmanuel J. Candès. *Conformalized quantile regression*. Curran Associates Inc., Red Hook, NY, USA, 2019.

[75] Victor Chernozhukov, Iván Fernández-Val, and Alfred Galichon. Quantile and probability curves without crossing. *Econometrica*, 78(3):1093–1125, 2010. doi:https://doi.org/10.3982/ECTA7880. URL https://onlinelibrary.wiley.com/doi/abs/10.3982/ECTA7880.

[76] JB Blair. Processing of NASA LVIS elevation and canopy (LGE, LCE and LGW) data products, version 1.0. *https://lvis. gsfc. nasa. gov*, 2018.

[77] Sander Riisøen Jyhne, Christian Igel, Morten Goodwin, Per-Arne Andersen, Serge Belongie, and Nico Lang. SuperF: Neural implicit fields for multi-image super-resolution. In Carl Vondrick, Bharath Hariharan, Colin Raffel, Lerrel Pinto, Diyi Yang, and Aleksandra Faust, editors, *International Conference on Learning Representations (ICLR)*, 2026. URL https://openreview.net/forum?id=FiiItlSqqL.

[78] Hao Tang, John Armston, and Ralph Dubayah. Algorithm theoretical basis document (atbd) for gedi l2b footprint canopy cover and vertical profile metrics. *Goddard Space Flight Center: Greenbelt, MD, USA*, 2019.

[79] K. M. Bergen, S. J. Goetz, R. O. Dubayah, G. M. Henebry, C. T. Hunsaker, M. L. Imhoff, R. F. Nelson, G. G. Parker, and V. C. Radeloff. Remote sensing of vegetation 3-d structure for biodiversity and habitat: Review and implications for lidar and radar spaceborne missions. *Journal of Geophysical Research: Biogeosciences*, 114(G2), 2009. doi:https://doi.org/10.1029/2008JG000883. URL https://agupubs.onlinelibrary.wiley.com/doi/abs/10.1029/2008JG000883.

[80] Wang Li, Wen-Yong Guo, Maya Pasgaard, Zheng Niu, Li Wang, Fang Chen, Yuchu Qin, Hailang Qiao, and Jens-Christian Svenning. Unmanaged naturally regenerating forests approach intact forest canopy structure but are susceptible to climate and human stress. *One Earth*, 7(6):1068–1081, June 2024. ISSN 2590-3322. doi:10.1016/j.oneear.2024.05.002. URL https://www.sciencedirect.com/science/article/pii/S2590332224002136.

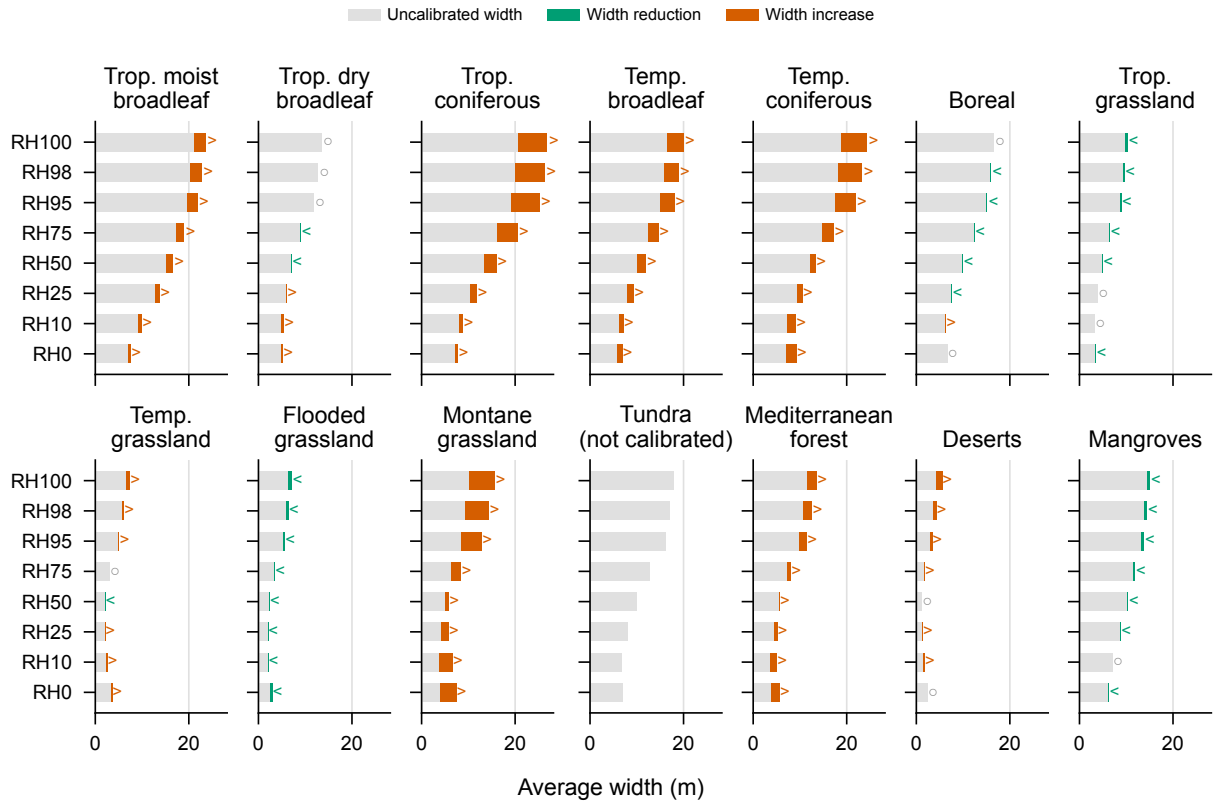
Appendix A Extended Data Figures and Tables

Filters	Description
quality_flag == 1	Indicating valid waveform
degrade_flag == 0	Non-zero values indicate the shot occurred during a degraded period.
region_class ≥ 0	Filter out water
leaf_off_flag != 1	The footprint has to be captured during leaf-on condition.
sensitivity ≥ 0.95	High sensitivity shots with high likelihood of reaching the ground in dense canopy covers.

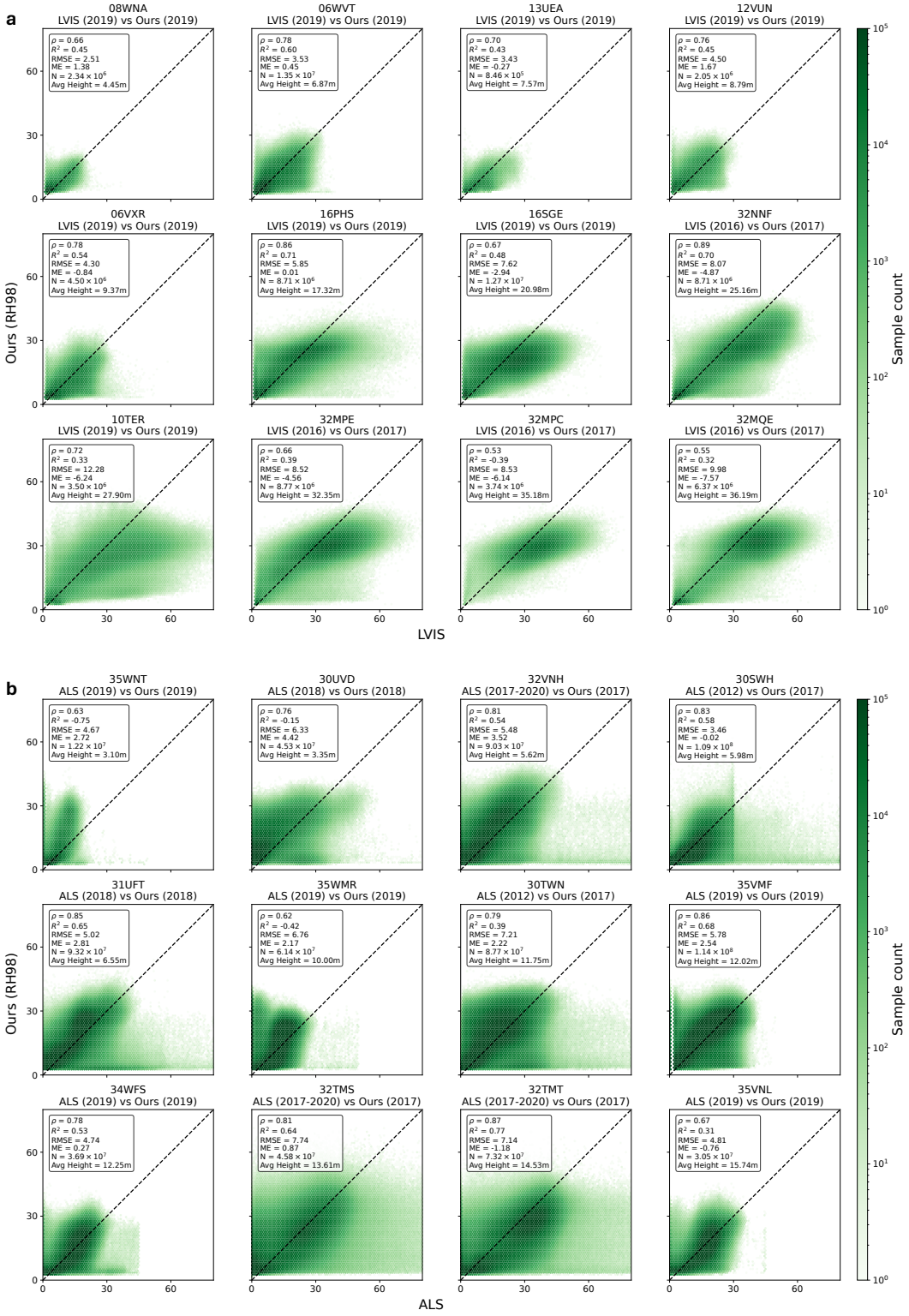
Extended Data Table A1: GEDI quality filters applied during sampling to retain high-quality, leaf-on footprints representative of vertical vegetation structure.

	R^2	RMSE (m)	ME (m)	Average height (m)	No. of points
LVIS	0.75	7.26	-2.69	20.47	$\sim$76 million
ALS	0.64	5.88	1.71	9.50	$\sim$800 million

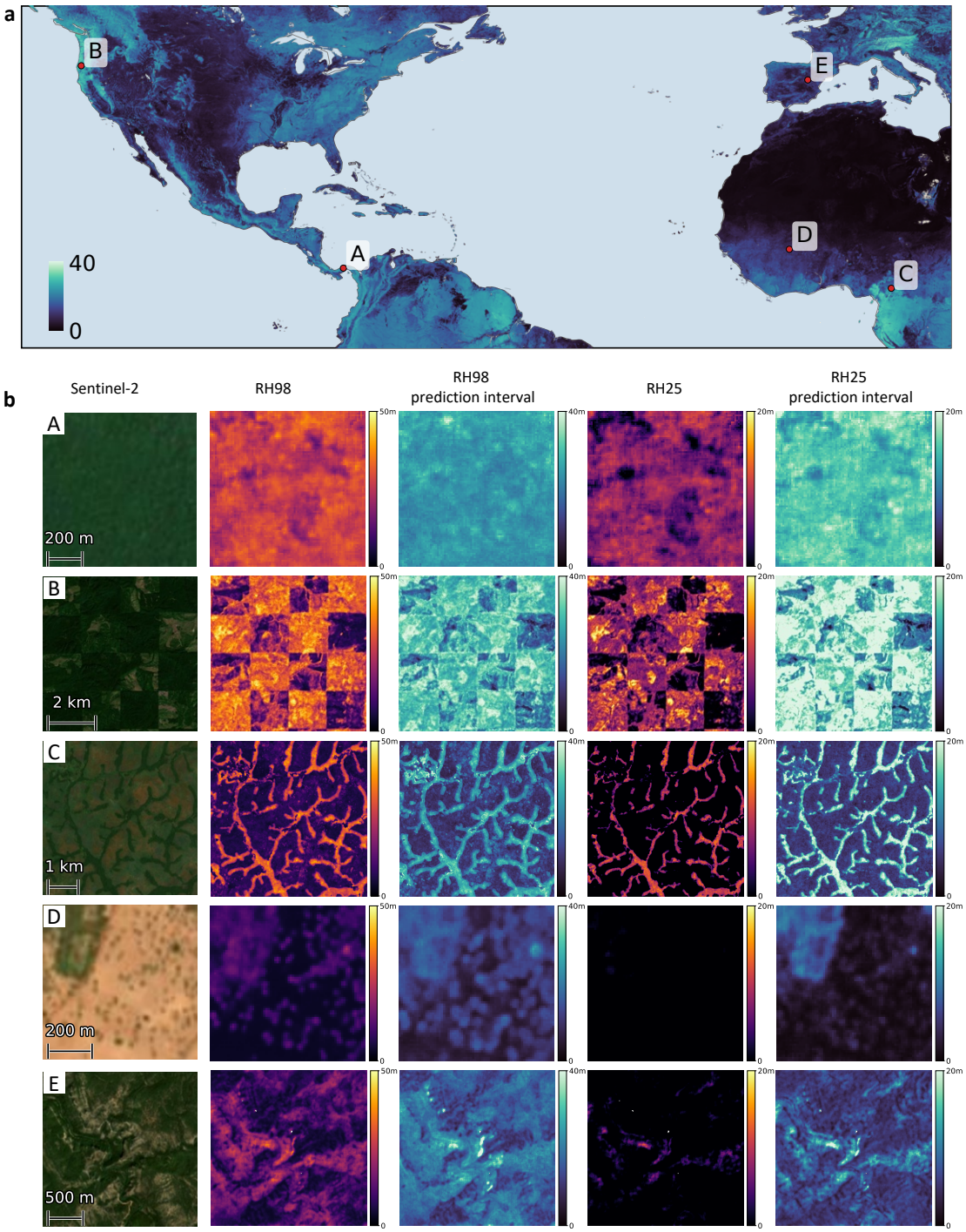
Extended Data Table A2: Evaluation of canopy top height estimates from VSM (RH98) against airborne laser scanning (ALS) and Land, Vegetation, and Ice Sensor (LVIS) reference data.



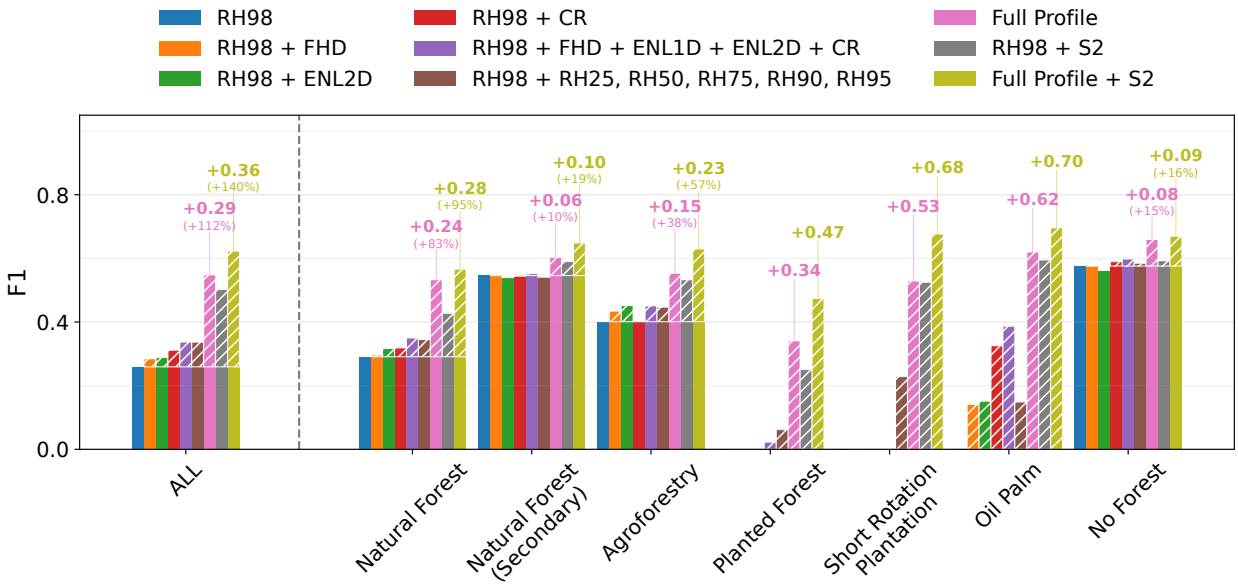
Extended Data Figure A1: Average prediction interval width per biome and RH metric before and after conformal calibration. Gray bars show the uncalibrated baseline width. A $<$ sign indicates a width reduction, with the green segment showing the magnitude; a $>$ sign indicates a width increase, with the orange segment showing the magnitude. ○ marks cases where calibration leaves the width unchanged. Tundra was excluded from calibration.



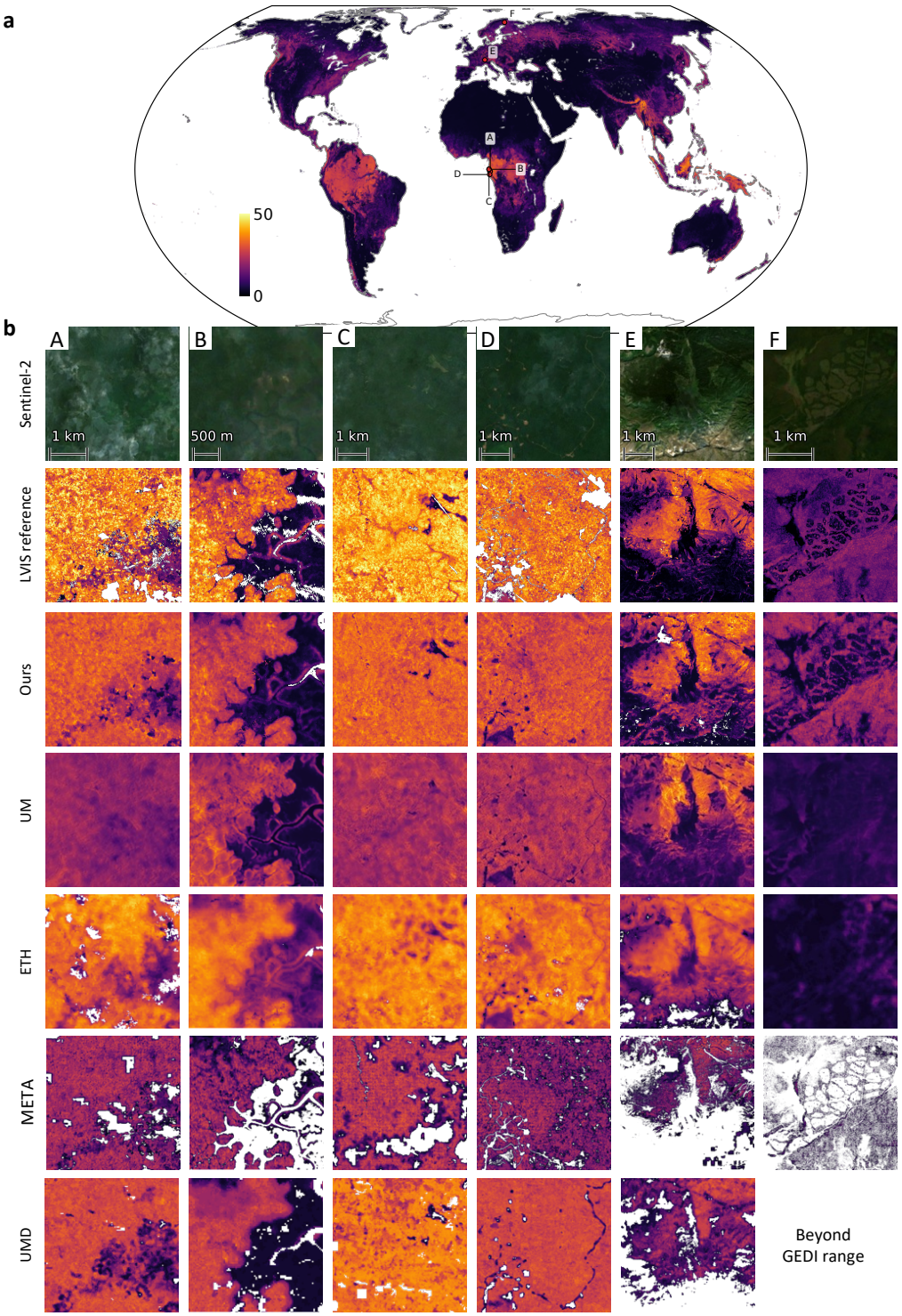
Extended Data Figure A2: **Predicted canopy top height overall agrees with independent airborne LiDAR across diverse geographic regions.** Density scatter plots comparing our canopy height estimates (RH98, y-axis) against independent airborne LiDAR reference data (x-axis) for **a,** 12 LVIS tiles across North and Central America and Africa, and **b,** 12 ALS tiles across Europe. Each scatter plot corresponds to a Sentinel-2 tile, with the acquisition years of the reference data and the corresponding prediction indicated in the title. Colour intensity indicates sample count on a logarithmic scale. The dashed line represents the 1:1 identity. Per-tile R^2, RMSE, ME, sample count (N), and average reference height are reported.



Extended Data Figure A3: Prediction intervals vary across different geographical regions and vegetation types, capturing distinct patterns of uncertainty. **a,** Global map of prediction intervals for RH98. **b,** Five example regions showing Sentinel-2 optical imagery, predicted RH98 and its prediction interval, and predicted RH25 and its prediction interval. Examples include tropical forest on Barro Colorado Island, Panama (A), harvesting patterns in Washington state, United States (B), gallery forests along rivers and ground water in Savannah landscapes, Cameroon (C), semi-arid Savannah in Koutiala, Mali (D), and Mediterranean vegetation, Spain (E). The prediction intervals exhibit spatial patterns that are not always correlated with canopy top height, for instance, uncertainty can be elevated in structurally heterogeneous areas where RH98 is low (E).



Extended Data Figure A4: **Forest naturalness and management classification benefits from horizontal and vertical structure information.** F1 scores across input feature combinations for logistic regression with spatial context, showing the added value of vertical structure information beyond canopy top height.



Extended Data Figure A5: **Our VSM provides canopy top height map that compares favorably with existing global products in terms of spatial detail and agreement with the reference data. a,** Canopy top height map (RH98) from VSM. **b,** Qualitative comparison of six example regions (A-F) against LVIS airborne LiDAR data (A-D) and ALS reference LiDAR data (E-F), alongside four existing global canopy top height products: UM[9], ETH[8], META version 1[50], and UMD[7]. The top row shows Sentinel-2 optical imagery for spatial context. The examples span dense tropical rainforest in Gabon and Cameroon (A–D), boreal forest in Finland (E), and temperate coniferous forest in Oregon, USA (F). Our map closely matches the spatial patterns in the reference data, though it exhibits slightly more underestimation of tall canopies compared to the ETH product. The UMD product is unavailable beyond the GEDI coverage range (column F). Canopy height ranges from 0 to 50 m.